UNIVERSITY OF HELSINKI REPORT SERIES IN ASTRONOMY

No. 500

Formation of bright central galaxies in massive haloes

Ghassem Gozaliasl

Academic dissertation

Department of Physics
Faculty of Science
University of Helsinki
Helsinki, Finland

To be presented, with the permission of the Faculty of Science of the University of Helsinki, for public criticism in the auditorium of A129 at Chemicum, Gustaf Hällströmin katu 2, 00560 Helsinki, on on the 22th of September at 12 o'clock..

Helsinki 2016

ISSN 1799-3024 (print version)
ISBN 978-951-51-2222-3 (print version)
Helsinki 2016
Helsinki University Print (Unigrafia)

ISSN 1799-3032 (pdf version)
ISBN 978-951-51-2223-0 (pdf version)
ISSN-L 1799-3024
http://ethesis.helsinki.fi/
Helsinki 2016
Electronic Publications @ University of Helsinki
(Helsingin yliopiston verkkojulkaisut)

Ghassem Gozaliasl: **Formation of bright central galaxies in massive haloes**, University of Helsinki, 2016, 100 p. + appendices, University of Helsinki Report Series in Astronomy, No. 500, ISSN 1799-3024 (print version), ISBN 978-951-51-2222-3 (print version), ISSN 1799-3032 (pdf version), ISBN 978-951-51-2223-0 (pdf version), ISSN-L 1799-3024

Classification (INSPEC): ABC1234
Keywords: galaxies, galaxy clusters, galaxy groups, fossil groups, galaxy evolution, galaxy formation LaTeX

Abstract

Galaxy formation and evolution is one of the most active and evolving fields of research in observational astronomy and cosmology. While we know today which physical processes qualitatively regulate galaxy evolution, the precise timing and behaviour of these processes and their relations to host environments remain unclear. Many interesting questions are still debated: "What regulates galaxy evolution? When do massive galaxies assemble their stellar mass and how? Where does this mass assembly occur?". This thesis studies the formation and evolution of central galaxies in groups and clusters over the last 9 billion years in an attempt to answer these questions.

Two important properties of galaxy clusters and groups make them ideal systems to study cosmic evolution. First, they are the largest structures in the Universe that have undergone gravitational relaxation and virial equilibrium. By comparing mass distributions among the nearby- and early-Universe clusters, we can measure the rate of the structure growth and formation. Second, the gravitational potential wells of clusters are deep enough that they retain all of the cluster material, despite outflows driven by supernovae (SNe) and active galactic nuclei (AGN). Thus, the cluster baryons can provide key information on the essential mechanisms related to galaxy formation, including star formation efficiency and the impact of AGN and SNe feedback on galaxy evolution. This thesis reports identification of a large sample of galaxy groups including their optical and X-ray properties. It includes several refereed journal articles, of which five have been included here.

In the first article (Gozaliasl et al. 2014a), we study the distribution and the development of the magnitude gap between the brightest group galaxies (BGGs) and their brightest satellites in our well defined mass-selected sample of 129 X-ray galaxy groups at $0.04 < z < 1.23$ in XMM-LSS. We investigate the relation between magnitude gap and absolute r-band magnitude of the central group galaxy and its brightest satellite. Our observational results are compared to the predictions by three

semi-analytic models (SAMs) based on the Millennium simulation. We show that the fraction of galaxy groups with large magnitude gaps increases significantly with decreasing redshift by a factor of ~ 2. In contrast to the model predictions, we show that the intercept of the relation between the absolute magnitude of BGGs and the magnitude gap becomes brighter as a function of increasing redshift. We attribute this evolution to the presence of a younger population of the observed BGGs.

In the second article (Gozaliasl et al. 2016), we study the distribution and evolution of the star formation rate (SFR) and the stellar mass of BGGs over the last 9 billion years, using a sample of 407 BGGs selected from X-ray galaxy groups at $0.04 < z < 1.3$ in the XMM-LSS, COSMOS, and AEGIS fields. We find that the mean stellar mass of BGGs grows by a factor of 2 from $z = 1.3$ to present day and their that stellar mass distribution evolves towards a normal distribution with cosmic time. BGGs are found to be not completely inactive systems as the SFR of a considerable number of BGG ranges from 1 to 1000 $M_{\odot}\ yr^{-1}$.

In the third article (Gozaliasl et al. 2014b), we study the evolution of halo mass, magnitude gap, and composite (stacked) luminosity function of galaxies in groups classified by the magnitude gap (as fossils, normal/non-fossils and random groups) using the Guo et al. (2011) SAM. We find that galaxy groups with large magnitude gaps, i.e., fossils ($\Delta M_{1,2} \geq 2$ mag), form earlier than the non-fossil systems. We measure the evolution of the Schechter function parameters, finding that M^* for fossils grows by at least +1 mag in contrast to non-fossils, decreasing the number of massive galaxies with redshift. The faint-end slope (α) of both fossils and non-fossils remains constant with redshift. However, ϕ^* grows significantly for both type of groups, changing the number of galaxies with cosmic time. We find that the number of dwarf galaxies in fossils shows no significant evolution in comparison to non-fossils and conclude that the changes in the number of galaxies (ϕ^*) of fossils are mainly due to the changes in the number of massive (M^*) galaxies. Overall, these results indicate that the giant central galaxies in fossils form by multiple mergers of the massive galaxies.

In the fourth article (Khosroshahi et al. 2014), we analyse the observed X-ray, optical, and spectroscopic data of four optically selected fossil groups at $z \sim 0.06$ in 2dFGRS to examine the possibility that they can be associated with diffuse X-ray radiation. The X-ray and optical properties of these groups indicate the presence of extended X-ray emission from the hot intra-group gas. We find that one of them is a fossil group, and the X-ray luminosity of two groups is close to the defined threshold for fossil groups. One of the groups is ruled out due to the optical contamination in the input sample.

In the fifth paper (Khosroshahi et al. 2015), we analyze data of the multi-

wavelength observations of galaxy groups to probe statistical predictions from the SAMs. We show that magnitude gap can be used as an observable parameter to study groups and to probe galaxy formation models.

Acknowledgements

I would first of all like to express my sincere gratitude to my supervisor, Prof. Alexis Finoguenov, for the continuous support of my Ph.D study and related research, for his positive energy, patience, motivation, and immense knowledge. His guidance helped me in all my time of research and writing of articles and this dissertation. I have acquired precious insights through his instructions, not only in academic studies but also enthusiasm in life.

My warm thanks goes to Prof. Habib G. Khosroshahi and Dr. Ali Dariush for turning my vision towards extragalactic astronomy and for supervising a part of my research. I would also like to thank Prof. Davood M.Z. Jassur, who supervised my early research into astrophysics.

My sincere thanks also goes to Docent Hannu Kurki-Suonio, who provided me an opportunity to join the Euclid team, and who financially supported a part of my work. I wish to thank Docent Syksy Rasanen and PAPU for the financial support of a part of my research and travel grants. I thank Prof. Guenther Hasinger and Dr. Mara Salvato for their advice and providing the foundation for the initial stages of my research at MPE in Garching. This work has been done in collaboration with several international colleagues. I thank them all for the valuable comments and feedback.

I warmly thank the preliminary examiners of this thesis, Dr. Angela Iovino and Dr. Dave Wilman, for their very helpful comments. I would like gratefully thank Dr. Charles C Kirkpatrick IV (Clif) for his help in editing the thesis. My grateful thanks goes to Prof. Chris Collins for taking on the role of the Opponent and my supervisor for acting as the Custos.

My thanks goes to Prof. Karri Muinonen, Docent Mika Juvela, Mr. Mikko Toriseva, Adj. Senior Scientist Mikko Sainio, Docent Jorma Harju, Assoc. Prof. Peter H. Johansson, Dr. Francesco Montanari, Dr. Kimmo Kettula, Dr. Tapio Lampen, Dr. Olli Wilkman, and Dr. Viola Allevato. I thank all my colleagues at the department and my office-mates, Mika and Erika.

This work has been supported by a grant of the Finnish Academy of Science to the University of Helsinki, decision number 266918. A part of this work has been supported by Helsinki Institute of Physics, School of Astronomy (IPM), and the German Deutsche Forschungsgemeinschaft, DFG Leibniz Prize (FKZHA1850/28-1).

I would like to thank my parents, brothers and sisters for supporting me spiritually throughout my life. I also thank my wife's parents, brothers and her sister for their kindly support.

Finally, my lovely thanks goes to my family, Fatemeh and Parisa. Without their valuable support and patience, it would not be possible to conduct this study.

Ghassem Gozaliasl

Helsinki September 2016

List of included publications

This PhD thesis contains six published and two submitted research papers (Gozaliasl et al. 2014a,b; Khosroshahi et al. 2014; Gobat et al. 2015; Khosroshahi et al. 2015; Gozaliasl et al. 2016). However, five papers are included here as follows:

Paper I: Gozaliasl, G., Finoguenov, A., Khosroshahi, H.G., Mirkazemi, M., Salvato, M., Jassur, D.M.Z., Erfanianfar, G., Popesso, P., Tanaka, M., Lerchster, M., Kneib, J.P., McCracken, H.J., Mellier, Y., Egami, E., Pereira, M.J., Brimioulle, F., Erben, T., and Seitz, S.: 2014. Mining the gap: evolution of the magnitude gap in X-ray galaxy groups from the 3-square-degree XMM coverage of CFHTLS. Astronomy and Astrophysics 566, A140.

Paper II: Gozaliasl, G., Finoguenov, A., Khosroshahi, H.G., Mirkazemi, M., Erfanianfar, G., and Tanaka, M.: 2016. Brightest group galaxies: stellar mass and star formation rate (paper I). Monthly Notices of the Royal Astronomical Society 458, 2762-2775.

Paper III: Gozaliasl, G., Khosroshahi, H.G., Dariush, A.A., Finoguenov, A., Jassur, D.M.Z., and Molaeinezhad, A.: 2014. Evolution of the galaxy luminosity function in progenitors of fossil groups. Astronomy and Astrophysics 571, A49.

Paper IV: Khosroshahi, H. G., **Gozaliasl, G.**, Rasmussen, J., Molaeinezhad, A., Ponman, T., Dariush, A. A., Sanderson, A. J. R.: 2014. Optically selected fossil groups; X-ray observations and galaxy properties. Monthly Notices of the Royal Astronomical Society 443, 318-327.

Paper V: Khosroshahi, H. G., **Gozaliasl, G.**, Finoguenov, A., Raouf, M., Miraghee, H.: 2015. Probing Galaxy Formation Models in Cosmological Simulations with Observations of Galaxy Groups. Publication of Korean Astronomical Society 30, 349-353.

Author's contribution to individual papers

- **Paper I (Gozaliasl et al. 2014a):**
  The author has the main responsibility of writing the paper and preparing figures. The author performs a comparison between the results in this study and the Adami et al. (2011) results, identifies galaxy groups, and carries out a statistical analysis of the magnitude gap between the first and the second brightest group galaxies. The author quantifies the effect of the contamination by dusty star forming galaxies on the red-sequence selection of group membership and compares the observational results with the predictions of SAMs. A. Finoguenov implements the X-ray analysis and determines the relation between the halo mass and the survey volume for groups. M. Mirkazemi runs the red-sequence finder and derives the colour-redshift relation of galaxies. Other co-authors provide comments on the results.

- **Paper II (Gozaliasl et al. 2016):**
  The author is responsible for writing the article and preparing all figures. The data analysis, script writing, plot fitting, and comparison with the SAM predictions are performed by the first author under direction of A. Finoguenov. M. Mirkazemi is responsible in writing §2.3. Other co-authors provide comments on the results.

- **Paper III (Gozaliasl et al. 2014b):**
  The author has the main responsibility for writing the article and preparing all figures. The author determines the composite luminosity function of galaxy groups and fits the Schechter function. H. G. Khosroshahi and A. Finoguenov supervise the article and A. Dariush also provides comments on the results, in particular, at early stage of analysis. Other co-authors give comments on the paper.

- **Paper IV (Khosroshahi et al. 2014):**
  H. G. Khosroshahi has the main responsibility of writing the paper and the X-ray analysis. The author is responsible for analysing the optical data, determining physical properties of all four galaxy groups and their brightest member galaxies, and computing the galaxy luminosity function. The author has the responsibility of writing section 4 and preparing all figures in this section. Other co-authors comment on the article contribute to the X-ray analysis.

- **Paper V (Khosroshahi et al. 2015):**
  The author contributes to sections 2 through 4 and preparing all figures. He has the responsibility of performing the magnitude gap statistics in both observations and models. He studies the galaxy luminosity function and its evolution with redshift using the Guo et al. (2011) model. H.G. Khosroshahi has the main responsibility of writing the article and other co-authors are responsible in providing Fig. 4. A. Finoguenov comments on the paper and supervises the writing of section 2 to 4.

List of abbreviations

2dFGRS	2dF Galaxy Redshift Survey
AEGIS	All-wavelength Extended Groth Strip International Survey
AGN	Active Galactic Nuclei
BCG	Brightest Cluster Galaxy
BGG	Brightest Group Galaxy
CFHT	Canada-France-Hawaii Telescope
CFHTLS	Canada-France-Hawaii Telescope Legacy Survey
CMD	Cold Dark Matter
CMB	Cosmic Microwave Background
COSMOS	Cosmic Evolution Survey
DM	Dark Matter
ESA	European Space Agency
FOF	Friend-Of-Friend
FOV	Field-of-view
HUDF	Hubble Ultra-Deep Field
HST	Hubble Space Telescope
IGM	Intragroup Medium
ICM	Intracluster Medium
ISM	Interstellar Medium
keV	kiloelectron volt
LSS	Large-Scale Structure
Λ CDM	Λ Cold Dark Matter
MS	Main Sequence
SAM	Semi-Analytic Model
SED	Spectral Energy Distribution
SDSS	Sloan Digital Sky Survey
sSFR	specific Star Formation Rate
SXDF	Subaru XMM-Newton Deep Field
SNe	Supernovae
SMBH	Super Massive Black Hole
SZ	Sunyaev-Zel'dovich
SXDS	Subaru/XMM-Newton Deep Survey
UDS	Ultra Deep Survey
XMM-LSS	XMM-Newton Large-Scale Structure Survey

Contents

1 Introduction

The present paradigm of structure formation within the framework of Λ cold dark matter (ΛCDM) cosmology predicts that large scale structure in the Universe forms via gravitational collapse due to strong primordial density fluctuation, then grows through a hierarchical sequence of accretion and mergers of smaller systems (e.g., White & Rees 1978; Springel et al. 2005; Kravtsov & Borgani 2012). Galaxy clusters are thus the most massive gravitational bound objects at the densest part of the large-scale structure of the Universe. They can be defined as nearly self-similar systems (Kaiser 1986).

Clusters and groups contain 50-70% of all galaxies in the local Universe (Geller & Huchra 1983; Eke et al. 2005) and the most massive galaxies, which are some 10 times more luminous than M^* galaxies (Collins et al. 2003). Although the light of member galaxies dominates the optical appearance of clusters, their contribution to the total baryonic mass is a small fraction, $\sim$5-15% (e.g., McCarthy et al. 2007; Dai et al. 2010). Observations show that clusters contain hot, X-ray emitting intracluster medium (ICM) that has been heated to temperatures up to several millions of degrees Kelvin (e.g., Finoguenov et al. 2007; Boehringer & Werner 2009). From the gravitational lensing effect, the dispersion in radial velocities of the galaxies within clusters, and X-ray detections, we are now able to estimate the total mass of the galaxy clusters. These measurements show that the baryon mass of clusters is $\sim$ 12-15% of the cluster total mass and the remaining fraction consists of dark matter. (e.g., Zwicky 1937; Vikhlinin et al. 2006; Giodini et al. 2012). The matter content of clusters is expected to be a fair sample of the matter in the Universe (e.g., White et al. 1993). As a tracers of the cosmic large-scale structure, they are used to test cosmological models, constraining the cosmological parameters (e.g., Vikhlinin et al. 2006; Boehringer & Werner 2009).

There is a general agreement among studies that galaxies in the early Universe do in fact form via dissipative collapse and merging of low mass galactic progenitors. Galaxies grow in stellar mass and size by accreting neighbor galaxies and matter from the surrounding haloes (e.g., Scoville et al. 2007; Conselice 2014). The brightest

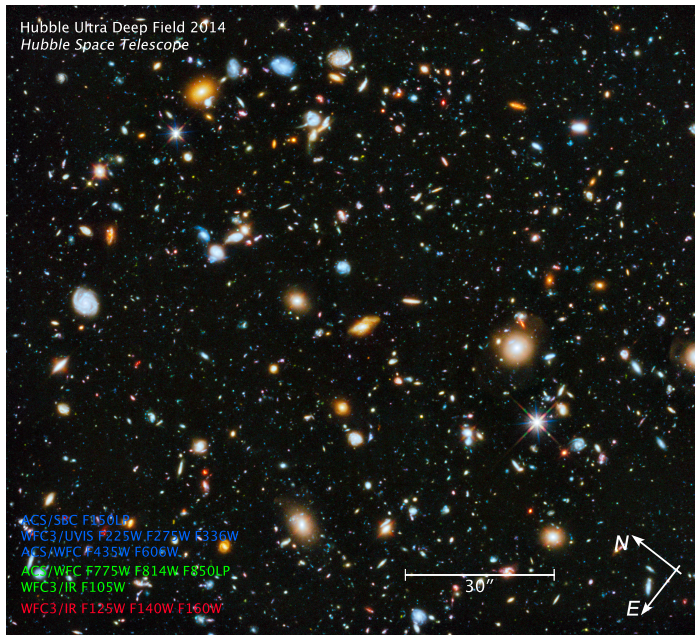

Figure 1.1: Deep imaging of galaxies down to magnitude 30 in the Hubble Ultra Deep Field survey (HUDF 2014), covering the whole range of wavelengths available to Hubble's cameras (ultraviolet through visible to near-infrared). The image shows galaxies with a variety of properties and morphologies distributed over the age of the Universe, $\sim$ 13 billion years (Credit: NASA, ESA, public domain).

group/cluster galaxies are the most unique examples of such process and the most massive, luminous galaxies to be formed.

The image of the full range of ultraviolet to near-infrared light of the Hubble Ultra-Deep Field (HUDF-2014), as shown in Fig. 1.1, indicates that galaxies exhibit a variety of physical properties. We observe that early Universe galaxies are bluer and more irregular and interacting than the nearby Universe galaxies, which have generally regular structures (e.g., Conselice 2014). Despite impressive observational findings and an understanding of what environmental and internal physical processes influence galaxy evolution, the precise behavior of the galaxy evolution mechanisms in the life of a galaxy are still elusive. This study aims to investigate the stellar mass assembly of BGGs and the impact of environment on BGG evolution over the last 9 billion years.

Groups are detected with a remarkable diversity of properties, in regard to rich-

ness, X-ray luminosity, temperature, and formation period. Observations indicate that mergers and galaxy interactions occur more frequently in groups because of their sufficiently high densities and low velocity dispersions that are essential for encounters (e.g., Ponman et al. 1994). The massive (M*) galaxies in normal groups are thought to gradually merge with the central galaxy, and eventually form a giant elliptical galaxy surrounded by faint satellites. A galaxy group that includes a luminous elliptical galaxy with an R-band magnitude gap of two or greater with the brightest satellite within half the virial radius of system and extended X-ray emission with a bolometric X-ray luminosity of $L_{x,bol} > 5 \times 10^{41}\ h_{70}^{-2}\ erg\ s^{-1}$ is known as a "fossil group". It is expected that fossil groups present a luminosity function with a deficit of M^* galaxies. In this thesis, we study the stacked luminosity function of galaxies in fossil and non-fossil groups down to an absolute magnitude of -15 and search for the link between formation of the central group galaxies and the evolution of the luminosity function below $z = 1$ using the Guo et al. (2011) SAM (Gozaliasl et al. 2014b).

The magnitude gap of groups, $\Delta M_{1,2}$, is used as an optical observable parameter to quantify the age of groups and to identify fossil groups (e.g., Ponman et al. 1994; Jones et al. 2003; D'Onghia et al. 2005; Dariush et al. 2007; Smith et al. 2010; Gozaliasl et al. 2014a; Raouf & Khosroshahi 2015; Raouf et al. 2016). The development of the magnitude gap of groups is believed to have a link with the merging of group galaxies (e.g., Jones et al. 2003; Dariush et al. 2007). This thesis extends the study of the magnitude gap distribution and its relation with the absolute (r-band) magnitude of the BGGs out to $z = 1.23$.

In addition, this dissertation aims to determine of the optical and X-ray properties of fossil galaxy groups and determine their luminosity function in absolute r-band magnitude using a sample of optically selected fossils at $z \sim 0.06$ in the 2dFGRS field. We examine the possibility that a galaxy group including a giant elliptical galaxy and a large magnitude gap can be associated with an extended X-ray emission, similar to that observed in fossil galaxy groups (Khosroshahi et al. 2014).

1.1 The structure of the dissertation

This dissertation includes five refereed journal articles and an introduction. The structure of this introduction is as follows. Chapter 2 discusses the general properties of galaxy groups, cluster mass measurements, identification of clusters and introduces the major survey data used here. Chapter 3 introduces the important physical processes that drive galaxy evolution. Chapter 4 discusses the distribu-

tion and evolution of stellar mass and star formation rate of BGGs. Chapter 5 presents a statistical study of the distribution and development of the magnitude gap and presents the properties of fossil groups. Chapter 6 studies the evolution of the stacked (composite) luminosity function of galaxies in group progenitors at $z < 1$ using the Guo et al. (2011) SAM. Chapter 7 summarizes our conclusions.

2 Identification and advantage of X-ray galaxy Groups

Groups of galaxies have a typical size of $D \sim 0.1 - 1\ h^{-1}$ Mpc and a typical mass (including dark matter and barons) of $\sim 10^{12}$ to $10^{14}\ M_{\odot}$. Cluster sizes typically span $D \sim 1 - 2\ h^{-1}$ Mpc and their total mass ranges from $\sim 10^{14}\ M_{\odot}$ up to $5 \times 10^{15}\ M_{\odot}$. They are rare structures compared to galaxy groups and the transition between groups and clusters is not sharp. The main distinction between them is made by richness and the velocity dispersion of the member galaxies. The richness is sensitive to depth and quality of observations. Groups and clusters typically consist of a few to hundreds of galaxies. The velocity dispersion of galaxies in groups and clusters range $\sim 200 - 400\ km\ s^{-1}$ and $\sim 400 - 1400\ km\ s^{-1}$, respectively (Postman & Murdin 2001; Schneider 2014).

Multi-wavelength observations, in particular in X-ray astronomy, explore the intracluster/intergroup X-ray emitting gas with $L_X \sim 10^{41} - 10^{44}\ erg\ s^{-1}$ and $T \sim 10^6 - 10^8\ K$ (e.g., Finoguenov et al. 2009; George et al. 2011). Fig. 2.1 shows an X-ray emitting cluster at $z = 0.731$ in COSMOS.

This chapter gives an overview on the X-ray emission from clusters, cluster red-sequence, and the methods for identifying clusters. Finally, we briefly describe the major data surveys used in this study.

2.1 The X-ray emission of groups and clusters

In recent years, most of the detailed knowledge on galaxy clusters has been established via X-ray observation. This is due to the fact that cluster gas has been heated up to $10^8\ K$ through the infall onto the gravitational potential wells of clusters. At this temperature, low density hot plasma ($\sim 10^{-3}$ atoms cm^{-3}) emits in the X-ray regime. The spectral energy distribution (SED) of the X-ray emission from ICM confirms that the X-ray radiation from clusters is mainly due to the thermal bremsstrahlung (free-free radiation). The emission that is generated when an elec-

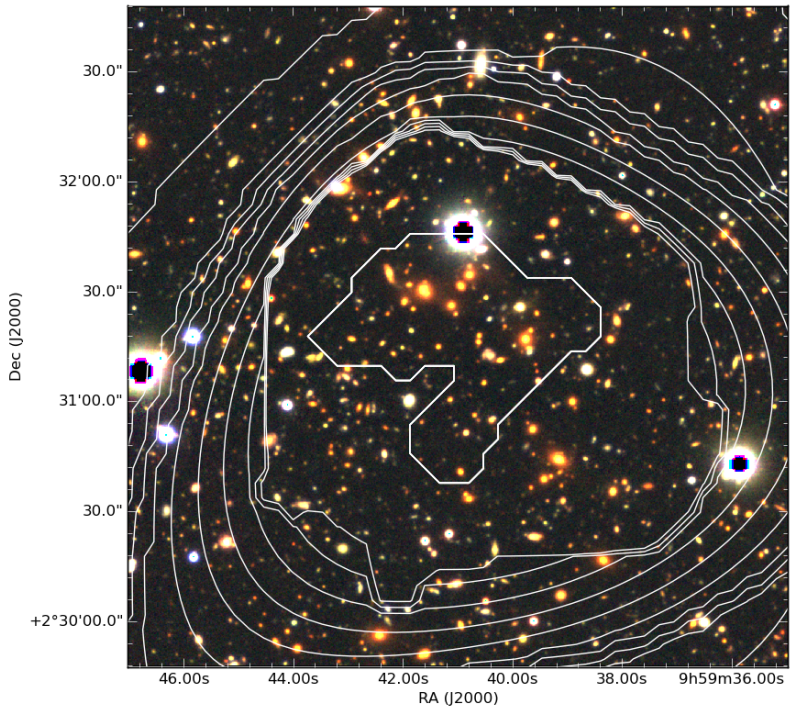

Figure 2.1: The combined g, r, and i band (Hyper Suprime-Cam) images of an X-ray galaxy cluster at $z = 0.731$ in the COSMOS field (Gozaliasl et al. in prep.). The white contours corresponds to the extended X-ray emission from the intracluster gas.

tron is accelerated in the electric field of an atomic nuclei (protons). The cluster gas mass is ~ 5 times the mass of the observable galaxies and stars, and its contribution to the total mass of clusters is about 5-25% (e.g., Vikhlinin et al. 2006; Giodini et al. 2012). X-ray observations provide a unique opportunity to measure precisely the total baryonic content of clusters, making them excellent tools to probe the matter content of the Universe (e.g. Ω_M) (Allen et al. 2004).

The following items summarize the important advantages of X-ray galaxy clusters.

- The X-ray emission guarantees the presence of a gravitational potential well that produces gravitational lensing effects (e.g., Hattori et al. 1999; Collins et al. 2003) .
- X-ray emission gives detailed information on the cluster mass distribution,

detection of the cool core or the non-cool core clusters, and the heating of cluster cores by the central AGN (e.g., Fabian & Nulsen 1977; Kaastra et al. 2004).

- X-ray spectroscopy gives detailed knowledge of the metallicity and chemical composition of the ICM (e.g., Böhringer & Werner 2010)

It has been established that the X-ray spectra of galaxy groups differ from those of clusters. Intra-group hot plasma has a lower temperature, thus the abundant elements are not fully ionised, and as a result, a fraction of the flux is due to line emission. The X-ray luminosity of galaxy groups generally range from $\sim 10^{41}$ to $10^{43}\ erg\ s^{-1}$. Galaxy groups exhibit a wide range of structure in terms of X-ray appearance. The low-mass groups generally show irregular X-ray shapes compared to the most massive groups and clusters with $L_X > 10^{43}\ erg\ s^{-1}$. In massive clusters, their central galaxies are generally located close to the peak of the X-ray radiation, while the diffuse X-ray emission from low-mass groups is generally distributed around several member galaxies and the central galaxies might not be close to the X-ray center.

The X-ray (e.g., mass) measurements are usually of at R_{500}, the radius within which the cluster mass density is 500 times the critical density. R_{500} corresponds to ~ 0.7 of the virial radius. Beyond this distance, the X-ray flux detection is difficult.

2.2 Red-sequence of cluster galaxies

Galaxy colour is used as an important redshift-dependent observable to study their evolution and to classify them as early- and late-type systems. Galaxies with a low contribution of hot, young stars (which radiate at high frequencies) appear red in colour. In contrast, galaxies with a high contribution of young stars appear blue.

The galaxy colour has a link with galaxy star formation activity. Blue colour galaxies are often active and star forming systems (e.g., spirals), while red galaxies are generally passive and quenched systems (e.g., ellipticals). Furthermore, red galaxies have a higher metallicity than blue ones.

Fig. 2.2 shows a schematic view of the relation between the colour and the luminosity (absolute magnitude) of SDSS galaxies, the so called galaxy colour-magnitude diagram (Bell et al. 2004). This digram consists of three main regions: red sequence, green valley, and blue cloud. The red sequence includes mostly red elliptical galaxies. The blue area contains blue spiral galaxies, and the green valley includes a number

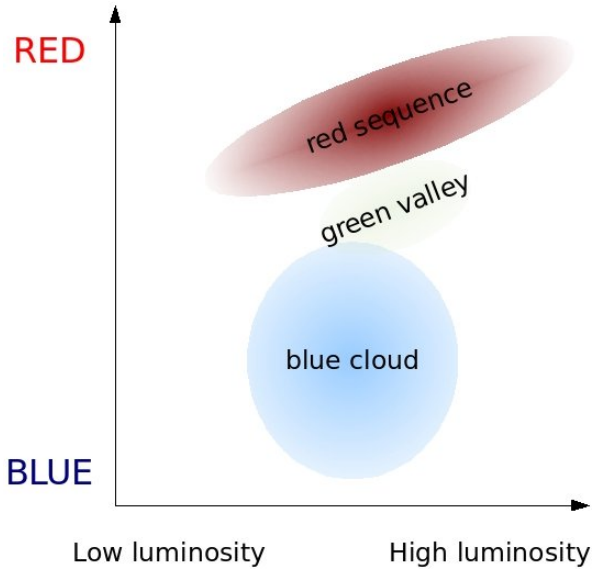

Figure 2.2: A schematic view of the galaxy colour-magnitude diagram with three populations: the red sequence, the blue cloud, and the green valley. The red sequence includes most red galaxies which are generally elliptical galaxies. The blue area contains most blue galaxies which are generally spirals, and the green valley includes a number of red spirals e.g., Milky way (Bell et al. 2004). (credit: CC BY-SA 3.0).

of red spirals (e.g., Milky way), indicating that colour parameters can differentiate galaxy populations remarkably well.

Since cluster galaxies experience similar effects and evolution, they exhibit similar colours. Thus, when we plot their well-defined colours (e.g., $r-i,\ z-i$) as a function of magnitude, they will fall on a roughly linear sequence known as the red-sequence (see lower panel of Fig. 2.3). The red-sequence is widely used for selecting group membership and for assigning a photometric redshift to galaxy groups (e.g., Koester et al. 2007; Mirkazemi et al. 2015).

In this thesis, we used a red-sequence finder (see Gozaliasl et al. 2014a; Mirkazemi et al. 2015) with two colours to assign group membership. We select a galaxy as a member of a group if its colours fall on both red-sequences of the hosting group (e.g., $g^{'}-r^{'}$ and $r^{'}-i^{'}$). The following combination of filters defined as a function of redshift for the red sequence algorithm: $0.05 \leq z \leq 0.66$: $g^{'}, r^{'},\ i^{'}$ and $0.66 < z \leq 1.10$: $r^{'}, i^{'},\ z^{'}$.

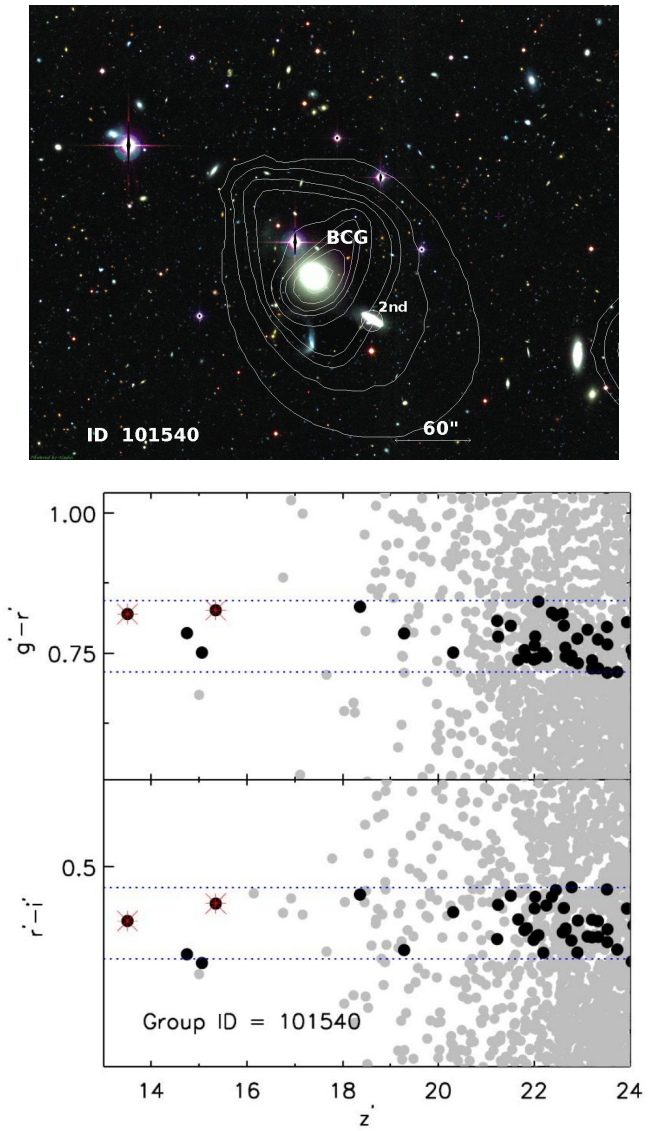

Figure 2.3: *Upper panel*: The combined CFHTLS r'-, i'-, and z'-band images with the overlaid X-ray emission contours of a fossil group candidate at $z = 0.07$. The two brightest group galaxies have been marked with white circles. *Lower panel*: Colour $g^{'} - r^{'}$ (upper) and $r^{'} - i^{'}$ (lower) as a function of $z^{'}$ magnitude. The dark circles illustrate group membership and two brightest group galaxy within $0.5R_{200}$ have been marked with red asterisks. The upper and lower limits of colours are shown by a horizontal dashed line. Figures are adopted from (Gozaliasl et al. 2014a).

2.3 Identification of galaxy groups and clusters

During the past 50 years, several techniques have been developed in order to identify galaxy groups. We briefly describe the most common methods as follows:

- *Detection of spatial over-densities:* the two most common methods to quantify the environment of a galaxy are the distance to the nearest neighbor (Dressler 1980) and the number of neighboring galaxies located within a fixed radius (Hogg et al. 2003). These measurements allow to identify over-densities. Clusters and groups are bound over-densities with $\rho/\bar{\rho} \geqslant 200$ (Berlind et al. 2006; Ramella et al. 2001).

- *Red-sequence method*: this method is widely used for detecting the over-density of the red galaxies. The 13,823 galaxy clusters in the MaxBCG catalogue have been identified using the red-sequence technique in SDSS (Koester et al. 2007). In paper I and paper IV, we use this technique to select group members (Gozaliasl et al. 2014a; Khosroshahi et al. 2014).

- *X-ray selection*: cluster of galaxies are the brightest extended sources in the X-ray sky. Thus, X-ray observations provide a unique opportunity for identification of clusters and groups. The X-ray selection is independent from the optical properties of galaxies. Catalogs of X-ray galaxy groups have already made an important contribution to studies of galaxy formation and evolution (e.g., Finoguenov et al. 2007; Finoguenov et al. 2009, 2010; Alshino et al. 2010; Erfanianfar et al. 2013; Gozaliasl et al. 2014a). In addition to cluster identification, modern X-ray surveys provide a precise cluster characterization.

- *Gravitational lensing method*: galaxy cluster work as lenses for the light rays of background galaxies. Thus, the lensing signal also provides powerful clues for identifying the foreground clusters or groups (e.g., Miyazaki et al. 2007).

- *Spectroscopic selection*: construction of a number of wide and deep galaxy redshift surveys (e.g. SDSS, 2dFGRS, and zCOSMOS) allows one to identify clusters using their spectroscopic redshift (e.g., Dressler et al. 1999; Gerke et al. 2012). The projection may affect $z < 0.1$ spectroscopic selection. However, at $z > 0.1$ the spectroscopic selections work well (e.g., Lilly et al. 2007).

- *Sunyaev-Zeldovich effect*: the energy of CMB photons moving through a galaxy cluster towards us can slightly boost during collision with hot electrons. Compton scattering transfers energy from the electrons to the CMB photons,

increasing on average the photon frequency after scattering. A consequence of this scattering is an increased number of high energy photons and a decreased number of photons at higher and lower energies, relative to the Planck spectrum. This effect is known as the Sunyaev-Zeldovich (SZ) effect (Sunyaev & Zeldovich 1970, 1972) and is observable. The SZ effect does not depend on the cluster redshift and the details of the gas distribution, offering a unique tool for studying the ICM (e.g., van de Voort et al. 2016) and to identify galaxy clusters (e.g., Reichardt et al. 2013; Bleem et al. 2015; de Haan et al. 2016).

In this study, we identify 129 X-ray galaxy groups at $0.04 < z < 1.23$ in CFHTLS W1 as a part of XMM-LSS (Gozaliasl et al. 2014a).

For identification of groups, we inspect the over-density of the projected galaxies to each extended X-ray source in the aforementioned surveys visually and determine the over-density of the projected galaxies in different redshift bins using their photometric and spectroscopic redshifts. In addition, we apply our red-sequence finder on each extended X-ray source to detect any red-sequence galaxies falling within a radius of about 500 *kpc* from the X-ray peak. This procedure is discussed in detail in Gozaliasl et al. (2014a); Mirkazemi et al. (2015).

In order to estimate the halo mass of the X-ray galaxy groups and clusters in our catalogue presented in the paper I (Gozaliasl et al. 2014a), we take into account the relation between the X-ray luminosity that we derive from the flux estimation and a total halo mass, inferred by the weak lensing analysis on systems of similar mass and redshift obtained in COSMOS field (Leauthaud et al. 2010). We also used the result of the study of the galaxy clustering (Allevato et al. 2012) to confirm the scaling relations used in this study.

2.4 COSMOS

COSMOS is the largest field ever observed using the HST. This survey covers ~ 2 deg^2 (a square with 1.4 degrees to a side). This survey was designed to probe the evolution and formation of galaxies as a function of both redshift and galaxy environments, while decreasing cosmic variance as a source of bias. The survey research goals and its features were presented in more details in Scoville et al. (2007).

This field has extensively been observed by several major ground- and space-based observatories, covering the full spectral range, with X-ray (Chandra and XMM–Newton), UV (GALEX), optical (Subaru), NIR (CFHT), near-infrared (UltraVISTA; ESO VISTA telescopes) mid-infrared (Spitzer), Herschel far-infrared (100, 160 μm), submillimetric (MAMBO) and radio (VLA) imaging. In addition, the X-

ray information provided by the 1.5 Ms exposure with XMM-Newton (53 pointings on the whole field, 50 ks each (Hasinger et al. 2007) and the additional 1.8 Ms exposure with Chandra in the central square degree (Elvis et al. 2009) allows robust detections of very high-z X-ray galaxy groups (e.g., Finoguenov et al. 2007; George et al. 2011).

COSMOS provides very deep (AB $\sim$ 25-27 mag) and multi-wavelength (0.23-24 μm) data of 2×10^6 of galaxies.

The COSMOS galaxies have also been observed by many spectroscopic programmes using different telescopes. The spectroscopic follow-up is still ongoing and includes the zCOSMOS survey at VLT/VIMOS (Lilly et al. 2007; Lilly et al. 2009), Galaxy Environment Evolution Collaboration 2 (GEEC2) survey with the GMOS spectrograph on the Gemini telescope (Balogh et al. 2011; Mok et al. 2013), Magellan/IMACS (Trump et al. 2007) and MMT (Prescott et al. 2006) campaigns, observations at Keck/DEIMOS (PIs: Scoville, Capak, Salvato, Sanders, Kartaltepe) and FLWO/FAST (Wright et al. 2010).

In this thesis, we used the X-ray data taken by both Chandra and XMM-Newton observatories, the optical images (e.g. Subaru, UltraVista, CFHTLS), and all spectroscopic data of galaxies. This data allows us to extend the detection of X-ray galaxy groups out to $z \sim 3$. We also use the previous catalogue of X-ray galaxy groups of this survey as presented in Finoguenov et al. (2009); George et al. (2011).

Fig. 2.4 shows the wavelet reconstruction of the early -type galaxy concentration in the photo-z catalogue of galaxies in the COSMOS field. The extended X-ray sources have been shown as green contours (Finoguenov et al. 2007).

2.5 CFHTLS

The CFHTLS observations were carried out in a period of 5 years between 2003 to 2008, covering a large area of $\sim$ 155 square degrees in four independent contiguous patches (known as W1, W2, W3, and W4). The CFHTLS photometric images were obtained in u*, g', r', i', z' bands with the MegaCam instrument. The point sources reach an 80% completeness limit in AB of $u* = 25.2$, $g' = 25.5$, $r' = 25.0$, $i' = 24.8$, and $z' = 23.9$. Within four fields, W1 is the largest field with 72 pointings that covers an area of $\sim$ 64 square degrees around $RA = 02h\ 18m\ 00s$, $Dec. = -07^\circ\ 00'\ 00''; s$, patch W2 includes 33 pointings around $RA = 08h\ 54m\ 00s$, $Dec. = -04^\circ\ 15'\ 00''$, patch W3 consists 49 pointings around $RA = 14h\ 17m\ 54s$, $Dec. = +54^\circ\ 30'\ 31''$ and patch W4 includes 25 pointings around $RA = 22h\ 13m\ 18s$, $Dec. = +01^\circ\ 19'\ 00''$ (e.g., Erben et al. 2013).

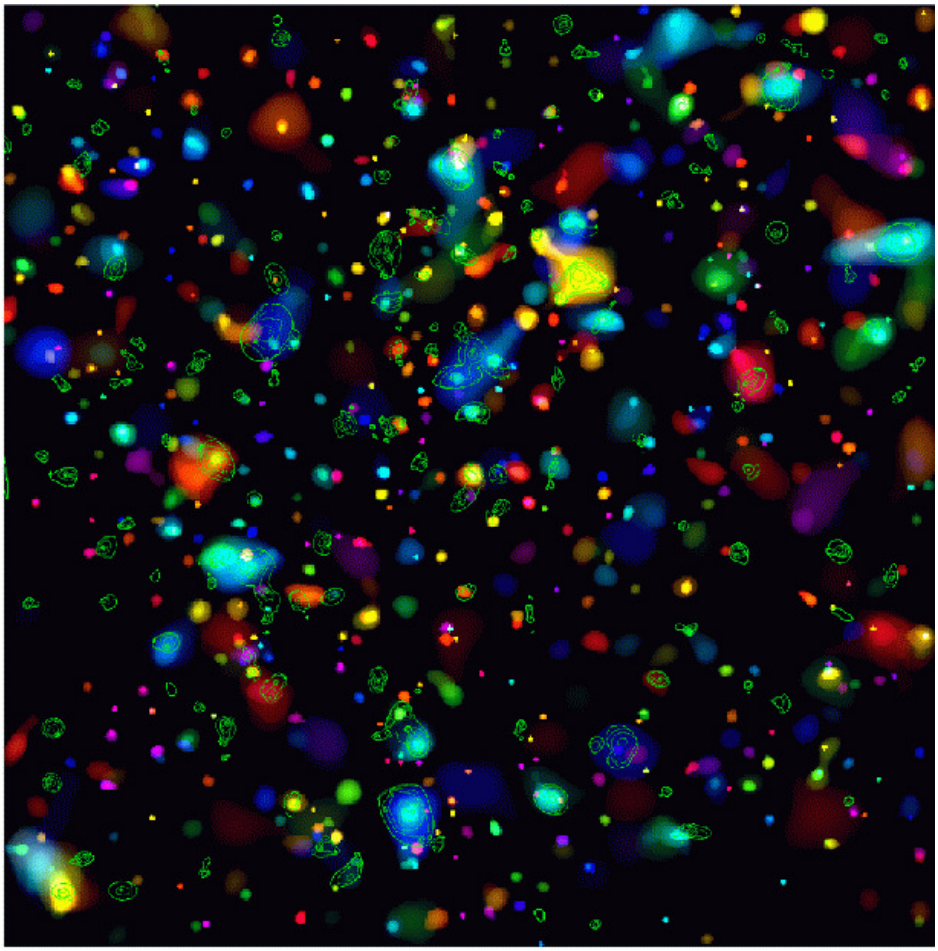

Figure 2.4: The colours of COSMOS. The wavelet reconstruction of the early-type galaxy concentrations searched in the photo-z catalog is colour-coded according to the average redshift: blue – 0.2, cyan – 0.4, green – 0.6, yellow – 0.8, red – 1.0. The green contours outline the area of the X-ray emission associated with 150 extended source candidates. The image is 1.5 degrees on a side. The pixel size is 10" on a side (Finoguenov et al. 2007).

The CFHTLS overlaps with several surveys such as COSMOS, XMM-LSS. In this thesis, we search for the X-ray galaxy groups using data of the CFHTLS together with data of X-ray observations of XMM-Newton in 3 deg^2 of XMM-LSS (Gozaliasl

et al. 2014a). We utilize the photometric redshift catalog of Brimioulle et al. (2008) in CFHTLS. CFHTLS has also a good spectroscopic coverage ~ 0.64 deg^2 with the VIMOS-VLT Deep Survey (VVDS; Le Fèvre et al. 2004, 2005) and the targeted cluster follow-up of Adami et al. (2011), which we also use in the present study.

2.5.1 AEGIS

We use data from the All-Wavelength Extended Groth Strip International Survey (AEGIS) located in CFHTLS W3 field, covering ~ 0.35 deg^2. The AEGIS data are used for studying the contamination of group members by dusty star forming galaxies when selecting the two brightest group galaxies using the two colour red-sequence finder. We utilise the AEGIS X-ray galaxy group catalogue (Erfanianfar et al. 2013) in the study of the stellar properties of the BGGs as presented in Gozaliasl et al. (2016).

3 Evolution of cluster galaxies

The schematic flowchart in Fig. 3.1 shows an overview of the physical processes that drive the evolution of a galaxy. Galaxies can accrete material through inflows from the ICM/IGM, and can lose matter through outflows driven by AGN, SNe, and environmental effects (e.g. tidal stripping of gas, mergers). Furthermore, several intergalactic physical processes and conditions contribute to the cooling of hot gas, converting cold gas to stars, and accreting of hot and cold gas onto the central black hole.

Observationally, it is not possible to trace galaxies backwards in time. We have thus sought to apply cosmological simulations for quantifying biases in observational data and interpreting observational findings. Towards this aim, several cosmological N-body simulations such as the Millennium simulation (e.g., Springel et al. 2005), SAMs (e.g., Bower et al. 2006; Guo et al. 2011; Henriques et al. 2015), and hydrodynamical simulations (e.g., Vogelsberger et al. 2014; McAlpine et al. 2016) have been constructed. We can now directly follow dark matter haloes, stars, and gas in entire galaxy populations in simulations. A successful model of galaxy formation is expected to predict a wide variety of observational scaling relations, such as the fundamental plane for elliptical galaxies, Tully-Fisher relation for spiral galaxies, tight relations between galaxy properties with its mass, central black hole mass, and halo mass. To achieve these goals, we are require to understand in more detail the physical processes that are responsible for galaxy evolution.

This chapter provides a brief introduction on the Millennium simulation and SAMs. Important physical properties and processes in the evolution and formation of galaxies are also defined.

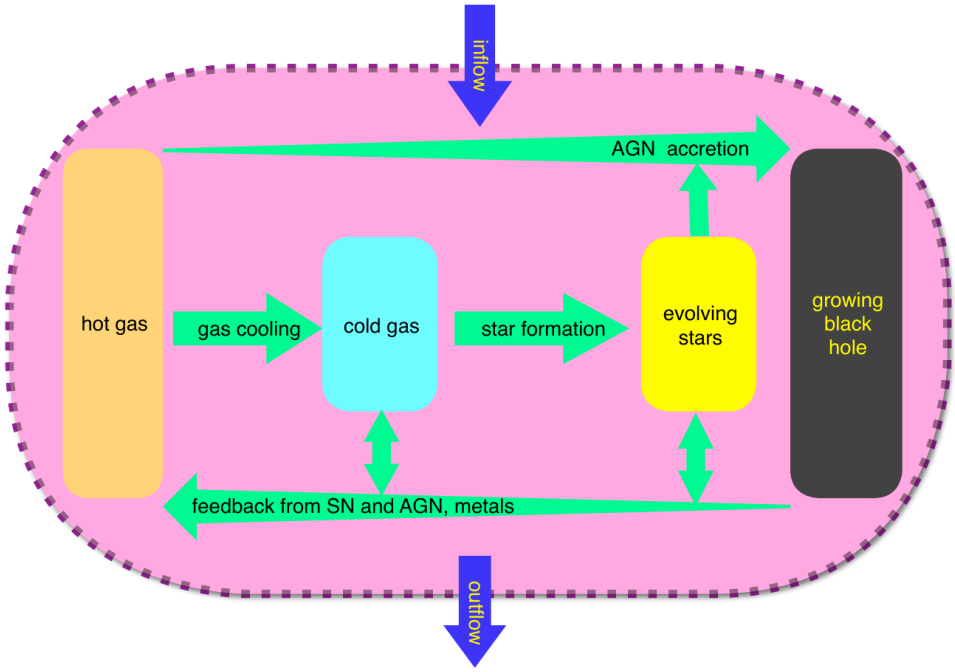

Figure 3.1: A schematic view of the evolution of an individual galaxy (dashed magenta box) which contains hot gas, cold gas, stellar population, and a black hole. The cooling process converts hot gas into cold gas, from which stars are formed. Through supernovae, energy, metals, and gas are ejected into the gas components. In addition, the central black hole grows by accretion of both cold and hot gas. This fuels the AGN and frees a large amount of energy which heats the gaseous components of the host galaxy. It is generally assumed the box to be open since gas can be accreted onto the galaxy from the IGM/ICM and can be ejected from galaxy through outflows driven by AGN and SNe feedback. Finally, a merger or interaction with another galaxy may also result in a significant boost or suppression of all these mechanism (Mo et al. 2010).

3.1 Millennium simulation and Semi-analytic models

3.1.1 Millennium simulation

The Millennium simulation was the largest cosmological N-body simulation based on the ΛCDM model published in 2005 (Springel et al. 2005). This simulation

was implemented using the cosmological parameters, (Ω_m, Ω_b, Ω_Λ, n, σ_8, h)=(0.25, 0.045, 0.75, 1, 0.9, 0.73), based on a combined analysis of the 2dFGRS (Colless et al. 2001) and the first-year WMAP data (Spergel et al. 2003). The Millennium simulation uses 2160^3 particles with typical masses of $1.18 \times 10^9\ M_\odot$ to trace the dark matter distribution in a cubic region 500 $h^{-1}\ Mpc$ on a side from redshift 127 to the present day. Application of simplified modeling techniques to the stored output of this simulation allows us to study the formation and evolution of the $\sim$ ten million galaxies more luminous than the Small Magellanic Cloud. In this simulation, the FOF algorithm was used to identify clusters and groups by linking particles with separation scale less than $\sim$ 0.2 the mean inter-particle separation (Davis et al. 1985). The identification of the sub-haloes in each FOF group is also performed by using the SUBFIND algorithm (Springel et al. 2001). The output of the Millennium simulation has been used several times in constructing SAMs such as Bower et al. (2006); De Lucia & Blaizot (2007); Guo et al. (2011); Henriques et al. (2015). For more details on the Millennium simulation, the reader is referred to Springel et al. (2005).

3.1.2 Semi-analytic model

In the last two decades, a number of simulation methods have been developed to give a statistical picture of galaxy formation and evolution history, in terms of specific star formation, stellar mass growth and halo mass assembly. The "semi-analytic model" method is the most economic and inexpensive technique that takes the approach of treating the different physical processes associated with galaxy formation in an approximate, analytic way.

Predictions from SAMs show good agreement with N-body/hydro calculations, but have been limited to either simulations of individual galaxies (e.g., Stringer et al. 2010) or simplified physics (e.g., Yoshida et al. 2003; Benson 2010).

Semi-analytic models are applied in order to study several aspects of galaxy formation such as galaxy counts, galaxy clustering, galaxy colours and metallicities, sub-mm and infrared galaxies, abundance and properties of Local Group galaxies, the reionization of the Universe, the heating of galactic disks, the properties of Lyman-break galaxies, supermassive black hole formation and AGN feedback (e.g., Bower et al. 2006; Croton et al. 2006; De Lucia & Blaizot 2007; Benson 2010; Guo et al. 2011; Henriques et al. 2015).

In this study, we use data from four SAMs (Bower et al. 2006; De Lucia & Blaizot 2007; Guo et al. 2011; Henriques et al. 2015). The main properties of these models have been summarized in Gozaliasl et al. (2014a).

3.2 Evolution processes

Several important processes contribute to the evolution of cluster galaxies and need to be included in implementation of the galaxy formation models such as SAMs. The important processes are briefly described here.

3.2.1 Gas cooling

Gas cooling is an important ingredient of galaxy formation. The rate of gas cooling depends on temperature, density, and chemical composition. Cooling of the hot gas occurs through a variety of mechanisms. At very high redshifts ($z > 6$), the density of CMB photons are high enough that the Compton scattering of these photons from electrons in the ionized ICM causes significant cooling of the host plasma. The CMB photon density is the same at any radius and independent from the gas density, thus Compton cooling timescale is independent of gas density (Peebles 1968; Benson 2010).

In massive haloes, where the virial temperature is $T_{vir} \sim 10^7\ K$, gas cools through Bremsstrahlung emission from free electrons. At a temperature range of $10^4\ K < T_{vir} < 10^6\ K$, transitions between energy levels excited by the collisions between electrons and partially ionized atoms become important in cooling process.

For haloes with $T_{vir} < 10^4\ K$, gas is expected to be neutral. In the presence of heavy elements or molecules, gas is unable to cool through the usual atomic processes. Cooling can occur by excitation of rotational or vibrational energy levels in molecular hydrogen through collisions (Bromm et al. 2009). The cooling of molecular hydrogen is more complicated compared to that of atomic cooling since there are still uncertainties in the details of molecular chemistry (Glover & Abel 2008).

3.2.2 Star formation

Based on observations, star formation mostly occurs in two modes: normal star formation and starbursts. The first is a consequence of cooling inflows and formation of a nearly self-gravitating disk in galaxies. These disks cool and become gravitationally unstable, and form massive stellar clouds, which themselves eventually lose their stability, fragment, and form stars. Starbursts are mostly limited to relatively small volumes (e.g., nucleus) of galaxies, which include a massive amount of gas. Observations reveal that they are triggered by strong interactions and instabilities. For instance, a significant merger can trigger a starburst in a galaxy. For a galaxy in starburst mode, the star formation rate can reach up to few thousands of solar masses per a year.

A number of studies indicate that the integrated star formation density in the Universe evolves significantly with redshift (e.g., Kennicutt Jr 1998; Leitherer et al. 1999; Daddi et al. 2007), rising from a low initial value at early epochs ($z > 6$) to a peak at $z \sim 2-3$, then decreasing to low values (e.g., Daddi et al. 2007; Wuyts et al. 2011). Daddi et al. (2007) show that for a given stellar mass, the star formation rate (SFR) at $z = 2$ is higher by a factor of ~ 4 and ~ 30 than that of star-forming galaxies at $z = 1$ and $z = 0$, respectively. They also found a tight correlation between SFR derived from UV/IR and stellar mass of galaxies in GOODS (at $z \approx 1$) in which massive galaxies have a higher star formation rates (Daddi et al. 2007; Noeske et al. 2007). A similar relation is also seen between SFR and stellar mass of the SDSS galaxies at $z = 0$, but with a lower normalization, indicating that the cosmic SFR density declines with cosmic time (e.g., Elbaz et al. 2007). There is also a tight relation between galaxy structure and SFR. High star forming galaxies are generally spiral types or those with central bright starburts (e.g., Conselice 2014). The SFR of galaxies strongly depends on the environment, as field galaxies are more star forming than cluster galaxies. The SFR is a key parameter that is used to classify galaxies into various categories of star forming/quenched systems (e.g., Van den Bergh 1976).

Unfortunately, the theory of star formation for different types of galaxies over cosmic time is not complete. Another important problem is that the contribution of different star formation modes to the stellar mass assembly of galaxies is not completely clear. In this thesis, we investigate the evolution and distribution of the SFR of the BGGs and compare our results with predictions from the SAMs based on the Millennium simulation.

3.2.3 Heating processes

Gas cooling and star formation in galaxies can be strongly suppressed by several heating processes. These processes are mainly driven by stellar evolution, growth of the central black hole of galaxies, and radiation from the first stars and quasars.

Supernovae and stellar winds: Observations of spectra (ultraviolet to infrared) of hot, luminous stars with masses above $\sim 15 M_{\odot}$ show that they undergo rapid mass outflows (stellar winds) that can erode their outer layers (De Jager et al. 1988). Furthermore, as the very massive stars die, a huge amount of mechanical and radiative energy are released by SN explosions. The SN-driven outflows can extend to even galactic scales and dramatically reheat, reshape, and ionize the surrounding interstellar medium (ISM) (e.g., Croton et al. 2006). In addition, they can even eject gas from the galaxy halo. Such effects are termed "SNe feedback". This feedback can have a significant impact on the evolution of galaxies, quenching their star formation

activities and changing their chemical composition (Larson 1974).

The cool cores of clusters and AGN feedback: The X-ray observations of galaxy clusters indicate that their ICM at the center of many clusters is very dense, thus the cooling time-scale becomes much shorter than the Hubble time-scale (e.g., Hudson et al. 2010; Fabian & Nulsen 1977). This finding led to the development of the cluster cooling-flow model. The model predicted that the ICM at the dense core of clusters quasi hydro-statically cools and the cooled gas is condensed under the weight of the surrounding ICM/IGM and dark matter halo. Consequently, the hot gas from the outer layers inflows to replace the condensed gas and a cooling-flow is produced. Accordingly, it was expected that a high amount of star formation must occur at the core of clusters, where the temperature of cooling gas falls to $10^4 K$. Later, this scenario was rejected by the optical observations of cluster cores (McNamara & O'Connell 1989). In addition, the X-ray spectroscopy of cluster cores with XMM-Newton (e.g., Tamura et al. 2001) indicate that the gas at these regions does not cool below one third of the virial temperature. This led to a conclusion that a heating source must be responsible in re-heating of the ICM and preventing further cooling of gas in cluster cores (Zakamska & Narayan 2003; Ruszkowski et al. 2004; Dennis & Chandran 2005; Mathews et al. 2006). AGN are possibly the main source of this heating (e.g., Bîrzan et al. 2004, 2008).

AGN are an important piece of the galaxy formation puzzle. They are believed to be powered by super-massive black holes with $L \sim 10^8 - 10^{14}\ L_\odot$. The AGN emission can change on timescales of a few days, indicating that this emission originates from a region of a few light days. Overall, $\sim$ 10-20% of energy radiated in the Universe comes from AGN. The energy released by an AGN can suppress the cooling flows of galaxies, thereby modifying the galaxy luminosities, colours, stellar mass, and quenching star formation activity.

3.2.4 Environmental effects

The structure and properties of galaxies strongly correlate with their local environments. Dressler (1980) studied galaxy morphology in 55 rich clusters and found that the number of elliptical and S0 galaxies (early type galaxies) increase as a function of increasing projected number density of galaxies, while the number of the spiral galaxies (or late type galaxies) decrease with increasing the galaxy number density. This correlation is known as "morphology-density relation". The morphology-density relation states that spiral galaxies are more common in the field (and in the lower density group environment). In contrast, elliptical (early-type) galaxies are more common in clusters.

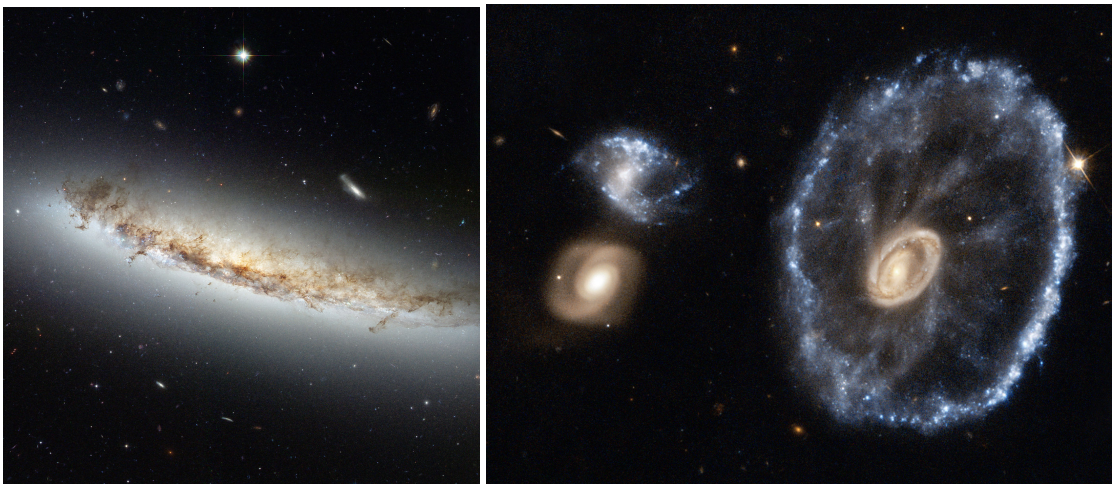

Figure 3.2: (*Left panel*) Ram pressure stripping of the gas from NGC 4402 in the Virgo Supercluster. The curved, or convex, appearance of the disk of gas and dust is a result of the forces exerted by the heated gas (credit: CC BY 3.0). (*Right panel*) The Cartwheel galaxy has recently been harassed, possibly due to an encounter with one of the two neighbouring galaxies (credit: PD-NASA).

As a result, the morphology-density relation indicates that environments affect the properties and structure of galaxies, particularly the star formation which is quenched once a galaxy falls within high density regions. There are several environmental processes (e.g., ram pressure stripping, tidal striping, and mergers) which must be taken into account in all galaxy formation theories.

Ram-pressure: When a satellite moves through the cluster, it experiences a wind due to its motion relative to the ICM. Ram-pressure removes some or all of the galaxy's ISM, suppressing star formation and even leading to a morphology transformation (e.g., Gunn & Gott III 1972). The left-panel of Fig. 3.2 shows an example of the ram-pressure gas stripping from the NGC 4402 galaxy in Virgo cluster.

Tidal gas striping: Tidal forces between cluster galaxies can remove gas from these systems and can even disrupt satellites. As a result, the stellar components, metals and cold gas of this satellite are then assigned to intracluster stellar population and the halo of central cluster galaxies. Gas stripping leads a rapid decline of star formation and reddening in the colours of the satellite galaxies (e.g., Kang & Van den Bosch 2008; Font et al. 2008).

Galaxy mergers: One of the most accepted views on the formation and growth

Figure 3.3: The two merging galaxies called NGC 2207 and IC 2163 in the distant Canis Major constellation (credit: PD-NASA).

of galaxies is that the most massive galaxies (e.g., BGGs/BCGs) form as a result of multiple mergers (e.g., Toomre 1977). When galaxy mergers occur, the structure of merging galaxies becomes very distorted and peculiar and the major galaxy undergoes an episode of intense star formation, the so-called "starburst ". This has been shown by numerical simulations (e.g., Springel & Hernquist 2005), as well as in observations (see right panel of Fig. 3.3) (e.g., Joseph & Wright 1985; Sanders & Mirabel 1996). For instance, at least 5 to 25 percent of galaxies in the Hubble deep field have been found to reveal signs of mergers. The galaxy merger rate is one of the most important and fundamental estimates of galaxy evolution. These measurements tell us how galaxies grow with time through encounters with other galaxies. Galaxy formation models based on ΛCDM define a merger tree, which describes the formation history of a dark matter halo and the associated galaxies.

Galaxy mergers are classified into two types: major and minor. The former one occurs between galaxies with masses differing by less than a factor of 3. If the mass ratio of merging galaxies exceeds this factor, the merger is assumed to be a minor merger. A major merger destroys the disks of the two merging galaxies and forms a spheroidal galaxy. But in a minor merger, the major galaxy's disk survives and accretes the cold gas and stellar contents of the small progenitor. Both mergers trigger a starburst which converts a fraction of the merging cold gas into stars. This

fraction of cold gas, e_{burst}, can be estimated by

$$e_{burst} = 0.56 \left(\frac{M_{minor}}{M_{major}} \right)^{0.7}, \tag{3.1}$$

where M_{minor} and M_{major} are the total baryonic mass of minor and major galaxies, respectively (Somerville et al. 2001; Cox et al. 2008; Somerville et al. 2008).

4 Evolution of the brightest group galaxies

It has been found that BCG luminosities are independent from the given global luminosity function (e.g., Tremaine & Richstone 1977). Von Der Linden et al. (2007) found, using a large sample of 625 BCGs in SDSS, that they have higher velocity dispersions and are larger than non-BCGs of the same stellar mass, indicating that they contain a higher fraction of dark matter. The dynamical mass-to-light ratio of BCGs does not change with galaxy luminosity and thus, they lie on a different Fundamental Plane compared to ordinary elliptical galaxies. The mean stellar ages and metallicity of BCGs are similar to non-BCGs of the same mass, but their α/Fe ratios are higher than non-BCGs, which shows that stars may have formed over a shorter time-scale in BCGs. Such findings suggest that formation of BCGs might be different from other elliptical galaxies.

Several scenarios have been suggested to describe the formation and evolution of BCGs. These include galactic cannibalism due to dynamical friction (e.g., White 1976a,b; Richstone & Malumuth 1983; Ostriker & Hausman 1977), tidal stripping from satellites (e.g., Richstone 1976; Merritt 1985), and star formation in cooling flow clusters (Fabian et al. 1994). Dubinski (1998) modeled galaxy cluster formation based on the ΛCDM model and showed that the central galaxy mainly forms due to early multiple mergers of several massive galaxies.

More recently, semi-analytic models assume two epochs of formation for BCGs. They consider that stars in BCG progenitors are initially formed by the collapse and condensation of cooling gas and gas-rich mergers at very early times, while later they continue to grow considerably through dry merging with old, red satellites (e.g., De Lucia & Blaizot 2007; Laporte et al. 2013). SAMs also assume that the gas cooling process in BCGs is reduced by heating, and AGN feedback at late times (e.g., Croton et al. 2006; Guo et al. 2011). Observations of X-ray cavities and radio cavities in clusters provide the strongest evidence for supporting the existence of AGN feedback.

Furthermore, numerical hydrodynamical simulations which include AGN driven buoyantly rising bubbles reproduce the observed stellar properties of BCGs remark-

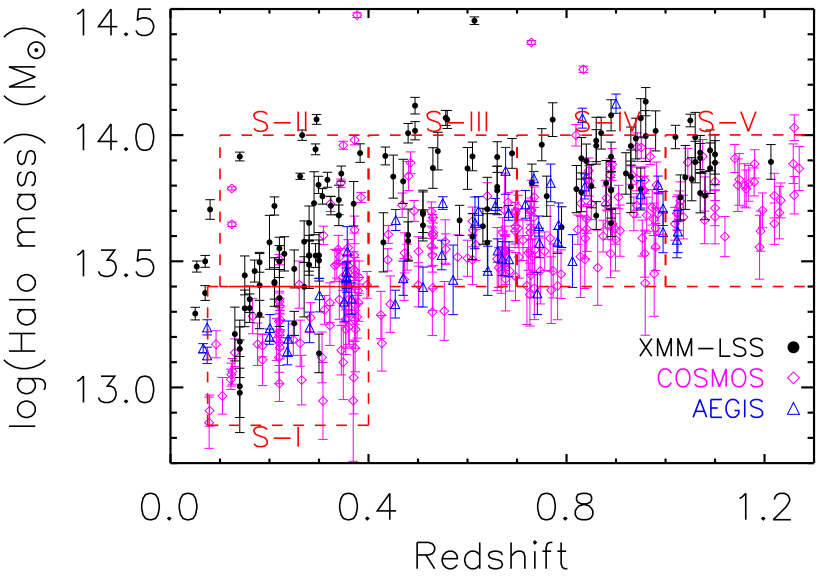

Figure 4.1: Halo mass (M_{200}) as a function of redshift for the X-ray galaxy groups selected from the COSMOS (open magenta diamonds), XMM-LSS (filled black circles), and AEGIS (open blue triangles) fields. The dashed red boxes illustrate our five defined subsamples. The figure is adopted from Gozaliasl et al. (2016).

ably well compared to models that do not include AGN feedback (e.g., Sijacki & Springel 2006). The growth of BCGs through dry mergers at late times is also largely in agreement with observations (Rines et al. 2007; Liu et al. 2009). However, some studies of the high-z BCGs disagree with this scenario (e.g., Whiley et al. 2008; Stott et al. 2010).

In this Chapter, we report our results on the distribution and evolution of the stellar mass and SFR of BGGs, and their relation with the halo mass using a large sample of BGGs at $0.04 < z < 1.3$. We select our sample of BGGs from X-ray selected galaxy groups with intermediate halo masses ($M_{200} = 10^{12.85}$ to 10^{14} $M_{\odot}$) where the group properties have been poorly investigated.

4.1 Data and sample definition

We use a large sample of 407 BGGs selected from X-ray galaxy groups in COSMOS (Finoguenov et al. 2007; George et al. 2011), XMM-LSS(Gozaliasl et al. 2014a), and AEGIS (Erfanianfar et al. 2013) fields.

Fig. 4.1 presents the halo mass of groups hosting BGGs versus redshift. We select five subsamples of X-ray galaxy groups considering their halo mass and redshift as follows:

S-I: 0.04 <z< 0.40 & $12.85 < log(\frac{M_{200}}{M_\odot}) \leq 13.50$

S-II: 0.10 <z≤ 0.4 & $13.50 < log(\frac{M_{200}}{M_\odot}) \leq 14.02$

S-III: 0.4 <z≤ 0.70 & $13.50 < log(\frac{M_{200}}{M_\odot}) \leq 14.02$

S-IV: 0.70 <z ≤ 1.0 & $13.50 < log(\frac{M_{200}}{M_\odot} \leq 14.02$

S-V: 1.0 <z≤ 1.3 & $13.50 < log(\frac{M_{200}}{M_\odot}) \leq 14.02$

Four subsamples (S-II to S-V) have a similar halo mass range. For these subsamples of BGGs, we can compare the BGG properties and their evolution over the last 9 billion years. This sample definition also allows us to compare properties of BGGs within haloes of different mass at the same redshift.

Over $\sim$ 200 BGGs in our sample have spectroscopic redshifts. The rest of the BGGs are likely selected using a red-sequence finder (Mirkazemi et al. 2015) with two colour selection and with a help of multiband photo-z. We use the galaxy photometric redshift catalogs of Ilbert et al. (2013); McCracken et al. (2012); Capak et al. (2007) in COSMOS, Brimioulle et al. (2008, 2013) in CFHTLS-W1, and Wuyts et al. (2011) in AEGIS. As shown in Fig. 4.2, we visually inspect the presence of the BGGs in the combined g, r, i-band images of their hosting groups.

We also use data from four SAMs presented in Bower et al. (2006, here after B06), De Lucia & Blaizot (2007, here after DLB07), Guo et al. (2011, here after G11), and Henriques et al. (2015, here after H15) for interpreting the observational results. In models, BGGs are selected from groups according to the halo mass and redshift range which we adopt in observations.

We present our results on the properties of BGGs in a series of three papers. The first paper has been published (bgg-paper I; Gozaliasl et al. 2016) and its main results will be discussed in the following sections.

Furthermore, in paper III (Gozaliasl et al. 2014b) we use the SAM of Guo et al. (2011) to study the evolution of the magnitude gap and the mass assembly of fossil and non-fossil groups. We first classify groups by the magnitude gap, putting them into three classes of normal/control groups ($\Delta M_{1,2} < 0.5$), fossil groups ($\Delta M_{1,2} > 2$),

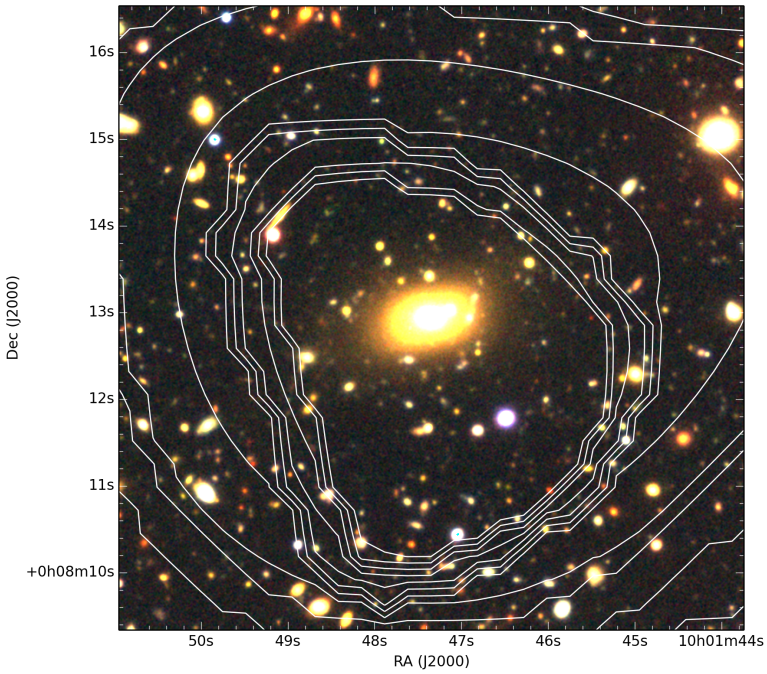

Figure 4.2: *(left panel)* The combined optical (g-, r-, and i-band) images of a galaxy group at $z = 0.322$ in the COSMOS field. The BGG is located at the X-ray centroid. White contours correspond to the X-ray emission from the IGM. The image is adopted from Gozaliasl et al. (2016).

and a sample of groups with random magnitude gap.

For each sample of these classes, we select three sub-samples following the halo mass and the BGG luminosity ranges:

(BS-I) $13.0 < log(M_{200}/h^{-1}M_{\odot}) \leq 13.5$ and $-22.5 < M_{r,BGG} \leq -22$,

(BS-II) $13.5 < log(M_{200}/h^{-1}M_{\odot}) \leq 14.0$ and $-23 < M_{r,BGG} \leq -22.5$, and

(BS-III) $14.0 < log(M_{200}/h^{-1}M_{\odot})$ and $-23.0 < M_{r,BGG} \leq -24.10$.

4.2 Star formation rate history

In the local Universe, star formation activity is strongly correlated to both local galaxy density and galaxy stellar mass (Brinchmann et al. 2004). Dressler (1980) found that massive early-type galaxies are located at high density regions and they

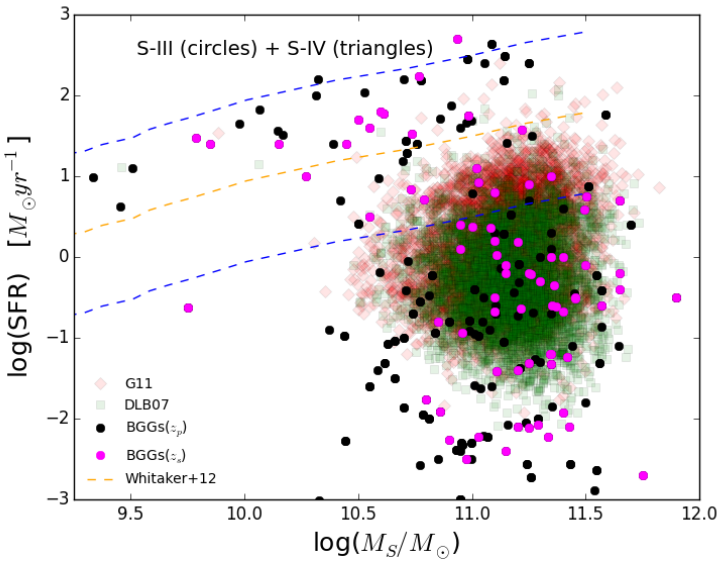

Figure 4.3: The SFR versus stellar mass of BGGs at intermediate redshift range between $0.4 \leq z \leq 1.0$. Magenta and black points represent the observed BGGs with spectroscopic and photometric redshifts, respectively. The dashed yellow line represents main sequence (MS) galaxies adopted from Whitaker et al. (2012). The dashed blue lines correspond to MS but with a ± 1 $M_\odot yr^{-1}$ shift in intercept. We select a BGG as a star forming/normal galaxy if its SFR falls between the two dashed blue lines. BGGs with lower SFRs are selected as passive systems. Red and green points present the $SFR - M_*$ relation in the SAMs of Guo et al. (2011) and De Lucia & Blaizot (2007), respectively. As a result, a considerable number of BGGs in observations fall in the main sequence, in contrast to the model predictions. The figure is adopted from Gozaliasl et al. (2016).

have generally been dominated by redder, older stars. The specific star formation rate (sSFR) (i.e., SFR per unit stellar mass) of galaxies is skewed towards lower values in denser regions (Brinchmann et al. 2004), indicating that more massive galaxies form stars at a lower rate per unit mass than low mass galaxies. Thus, the stars in massive galaxies should be formed at earlier times compared to the stars in low mass galaxies (Thomas et al. 2005). The presence of quenched and red galaxies is difficult to reproduce unless AGN feedback is introduced. While we know today that several processes affect star formation in galaxies, the star formation history of

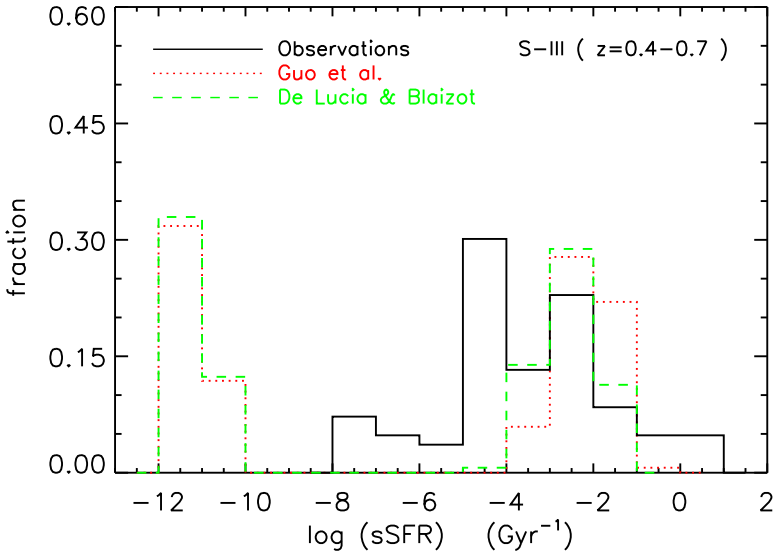

Figure 4.4: Distribution of specific SFR of BGGs. Models underestimate significantly the fraction of star forming BGGs. The figure is adopted from Gozaliasl et al. (2016).

massive galaxies is still not fully understood.

Recent observational studies indicate that the SFR of BGGs/BCGs is not always low (e.g., O'dea et al. 2008; Pipino et al. 2009; McDonald et al. 2011; Liu et al. 2012; Oliva-Altamirano et al. 2014). In particular, local Universe BGGs harbour ongoing star formation with rates up to 10 $M_{\odot}\ yr^{-1}$, having important implications on model predictions (e.g., Tonini et al. 2012; Oliva-Altamirano et al. 2014).

In paper II (Gozaliasl et al. 2016), we used the SED fitting method (le Phare code) and estimate the physical properties (e.g. stellar mass, SFR) of BGGs. We investigate the distribution of the sSFR of BGGs and probe the evolution of the average SFR of BGGs over the last 9 billion years. We also determine the SFR-stellar mass relation and the sSFR-halo mass relation.

Fig. 4.3 presents the relation between SFR and stellar mass of BGGs at intermediate redshifts $0.0 < z < 1.0$ in observations (black circles (BGGs with photo-z) and magenta circles (BGGs with spec-z)) and in the SAMs of Guo et al. (2011) (red points) and De Lucia & Blaizot (2007) (green points) in the SFR range of $-3 < log(SFR/M_{\odot}\ yr^{-1}) < 3$. In order to identify star forming and non-star forming BGGs, we adopt the main sequence relation of galaxies presented in

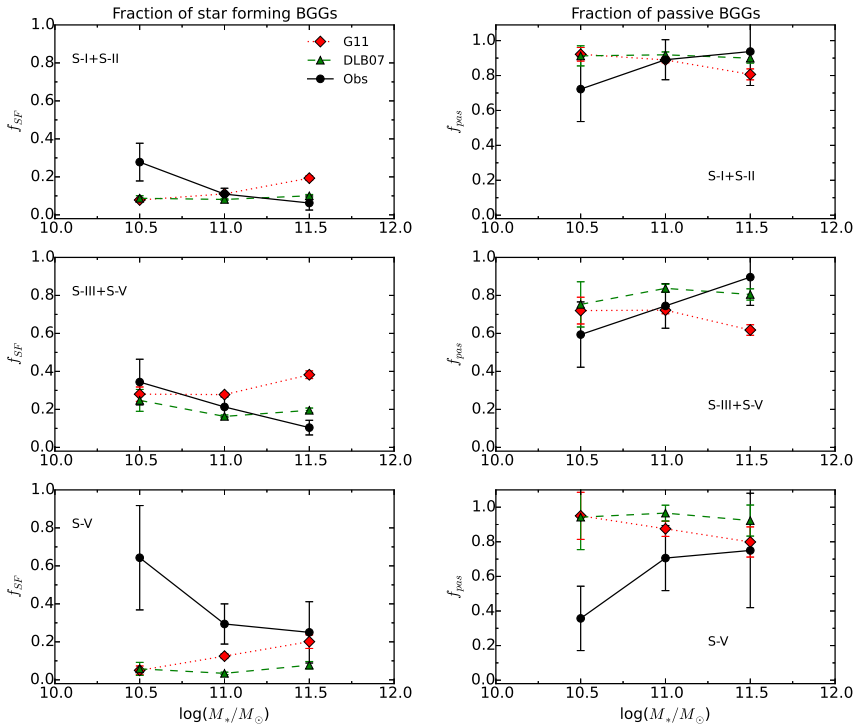

Figure 4.5: The fraction of star forming (left hand panels, f_{SF}) and passive (right hand panels, f_{pas}) BGGs as a function of the stellar mass of BGGs for S-I+S-II (upper panel), S-III+S-IV (middle panel), and S-V (lower panel). The solid black line, dotted red line, dashed green line illustrate the trends in observations and the G11 and DLB07 models, respectively. The figure is adopted from Gozaliasl et al. (2016).

Whitaker et al. (2012) (dashed yellow line). The dashed blue lines corresponds to $log(SFR/M_\odot\ yr^{-1}) \pm 1$ for a given stellar mass. If a BGG SFR falls between the two blue lines, we select it as a star forming BGG. As seen in Fig. 4.3, there are a considerable number of BGGs with SFR of 1 to 1000 $M_\odot\ yr^{-1}$, showing that BGGs are not entirely quenched systems.

Fig. 4.4 shows the distribution of the sSFR of BGGs for S-III. In contrast to

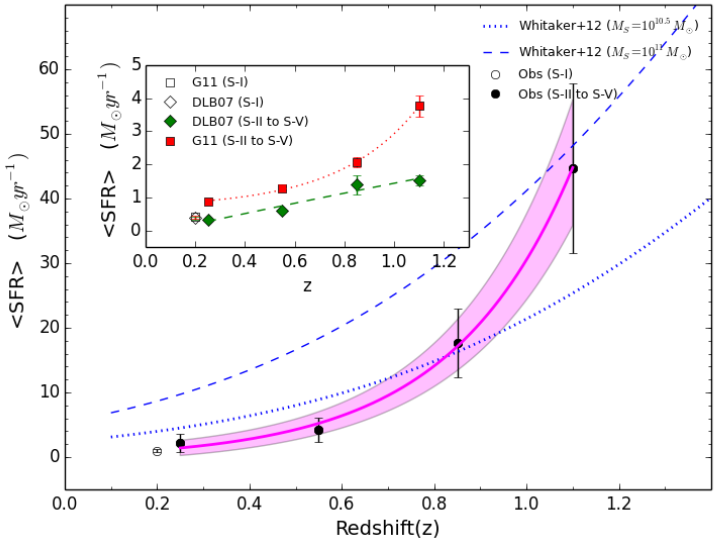

Figure 4.6: The redshift evolution of the average SFR of BGGs in observations (black circles). The magenta line and the highlighted area represent the best-fitting relation and its 68 per cent confidence intervals. The dashed and dotted lines represent SFR evolution for galaxies with M_*=$10^{10.5}$ and 10^{11} $M_\odot$ in the study of Whitaker et al. (2012), respectively. The subplot shows the redshift evolution of the mean SFR of the BGGs in the G11 (dotted red line) and DLB07 (dashed green line) models, respectively. The average SFR of BGGs is found to increase significantly with increasing redshift in observations. The figure is adopted from Gozaliasl et al. (2016).

observations, we find that at least 50% of BGGs in models exhibit no star formation activities. In order to quantify this discrepancy, we classify BGGs into two types of star forming/normal and passive systems using the main sequence of Whitaker et al. (2012) and study the fraction of passive/star forming BGGs as a function of stellar mass. The left-hand and right-hand panels of Fig. 4.5 present the fraction of star forming BGGs (f_{SF}) and the fraction of passive BGGs (f_{pas}) as a function of their stellar mass for S-I to S-V, respectively. For all subsamples of BGGs, we find that the fraction of star forming BGGs decreases as a function of increasing stellar mass with a corresponding increase of the fraction of passive BGGs. Models fail to reproduce the observed trend for BGGs at $1 < z < 1.3$ (S-V).

In Fig. 4.6, we explore the evolution of the average SFR of BGGs in observations (black points) at $0.04 < z < 1.3$. The trend in observations is approximated by the following best-fitting relation (the solid magenta line)

$$< SFR >= (0.70 \pm 0.06)e^{(3.79\pm0.10)z} + (-0.39 \pm 0.97) \quad (4.1)$$

We find that the mean SFR of BGGs grows significantly with increasing redshift. Since models show no significant evolution of BGG SFR, we illustrate the $SFR - z$ relation in models separately.

The dotted and dashed blue lines in Fig. 4.6 shows the SFR evolution of galaxies for two given stellar masses, $log(M_*/M_\odot) = 10.5$ and 11, in the study of (Whitaker et al. 2012). The SFR of our BGGs does not deviate significantly from the SFR of galaxies of the same stellar mass.

In Gozaliasl et al. (2016), we also find that the low mass BGGs in low-mass haloes are more active in forming stars than BGGs in more massive haloes over the same redshift range. The sSFR of BGGs within low-mass haloes (S-I) is found to decrease as a function of increasing halo mass at $z < 0.4$.

4.3 Stellar mass assembly

In the hierarchical framework of structure formation in the Universe, galaxies build up their mass by converting the accreted cold gas from the surrounding halo into stars and through merging with other galaxies. SAMs are constructed on the standard model of ΛCDM prediction that BCGs grow substantially with redshift. For instance, De Lucia & Blaizot (2007) found that the BCG stellar mass in their SAMs can increase up to a factor of 4 since $z = 1$.

Observational studies have presented conflicting results, mainly claiming little or no growth of the stellar mass in BCGs (e.g., Whiley et al. 2008; Collins et al. 2009; Stott et al. 2010). Aragón-Salamanca et al. (1998) used a sample of optically selected clusters and showed that the stellar mass of BCGs increases by a factor of 4 between $z = 1$ and present day. In contrast, using an X-ray-selected cluster sample at a similar redshift range ($z < 0.8$), Burke et al. (2000) found no significant growth for the BCG stellar mass.

One of the main goals of the present study is to take advantage of a large sample of X-ray selected groups with intermediate halo masses $\sim 10^{13} - 10^{14}$ $M_\odot$ in order to investigate the stellar mass evolution from $z = 0.04$ to 1.3 (Gozaliasl et al. 2016). For the first time, we inspect the evolution of the stellar mass distribution relative to a normal distribution. In Fig. 4.7, we show the stellar mass distribution of BGGs

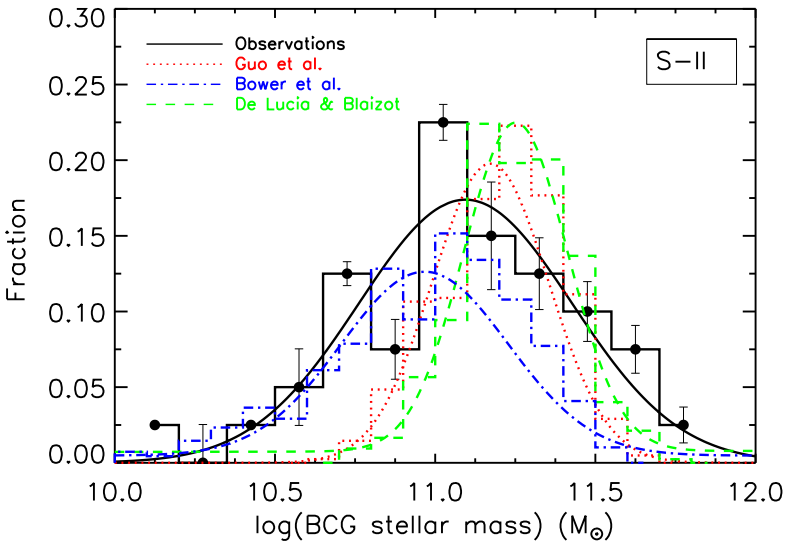

Figure 4.7: The stellar mass distribution of BGGs within groups with $M_{200} = 10^{13.5}$ to $10^{14} M_{\odot}$) spanning the redshift range of $0.1 < z < 0.5$ in observations (black histogram) and the SAMs (colour histograms). The best-fit of the Gaussian function to the data in observations and models are shown with solid black, dotted red (G11), dashed (DLB07), and dash-dotted (B06) lines, respectively. The figure is adopted from Gozaliasl et al. (2016).

for S-II in observations (black histogram) and in SAMs (colour histograms). We fit a Gaussian function to the data and quantify this distribution. As a result, we find evidence for the presence of a second peak at lower masses around $\sim 10^{10}$ $M_{\odot}$ and show that the shape of the observed mass distribution deviates from that of a normal distribution with increasing redshift, in contrast to the SAM predictions. This distribution skews to low masses with increasing redshift (see Fig. 3 and Fig. 4 in Gozaliasl et al. (2016)).

In Gozaliasl et al. (2016), we also show that the average stellar mass of BGGs grows by a factor of 2 since $z = 1.3$, which is in good agreement with resent results (e.g., Lidman et al. 2012; Lin et al. 2013) and the SAM predictions (see Fig. 4.8). This growth can be explained by multiple mergers of BGGs with nearby satellites. In addition, we also find evidence that the growth of the stellar mass of BGGs slows down at $z < 0.5$, in agreement with the recent results from Bellstedt et al. (2016).

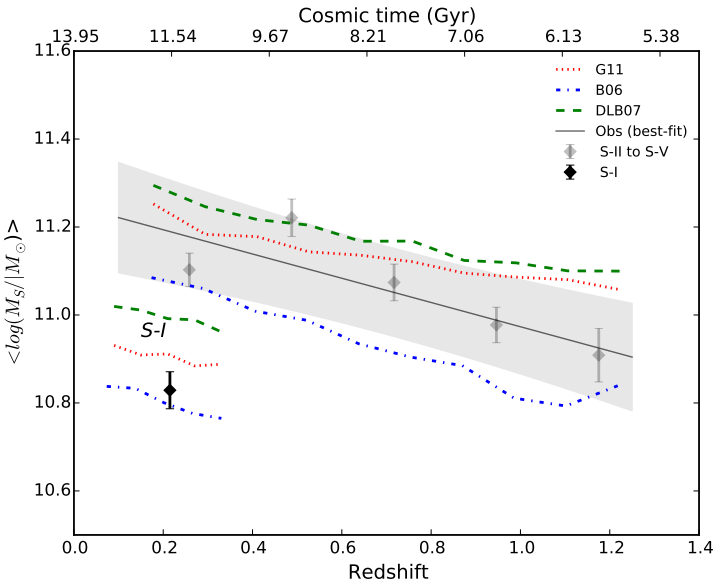

Figure 4.8: The average stellar mass of BGGs as a function of redshift (gray points). The solid black line and highlighted area represent the best-fit of the linear relation to the data and its 68 per cent confidence interval. The dashed green, dotted red, and dash-dotted blue lines present the mean stellar mass evolution in the SAMs of Bower et al. (2006); De Lucia & Blaizot (2007); Guo et al. (2011), respectively. In agreement with models, the average stellar mass of BGGs increases by a factor of ~ 2 since $z = 1.3$ to today. the figure is taken from Gozaliasl et al. (2016).

4.4 The stellar mass and halo mass relation

Environment plays a key role in the formation of BCGs because of their special location in the cluster. Several authors have identified a correlation between BGG properties (e.g., luminosity, stellar mass) and the halo properties (e.g., X-ray luminosity, mass) (e.g., Brough et al. 2002; Nelson et al. 2002; Whiley et al. 2008; Sanderson et al. 2009; Ascaso et al. 2011).

There is a well-known relation between the stellar mass of BCGs and the halo mass of clusters. This relationship suggests that the more massive BCGs are found in more massive haloes. The slope of this relation is less than unity, indicating that BCGs grow with rates which are slower than the rate of the growth of hosting clusters (Aragón-Salamanca et al. 1998; Brough et al. 2002; Brough et al. 2005, 2008; Stott

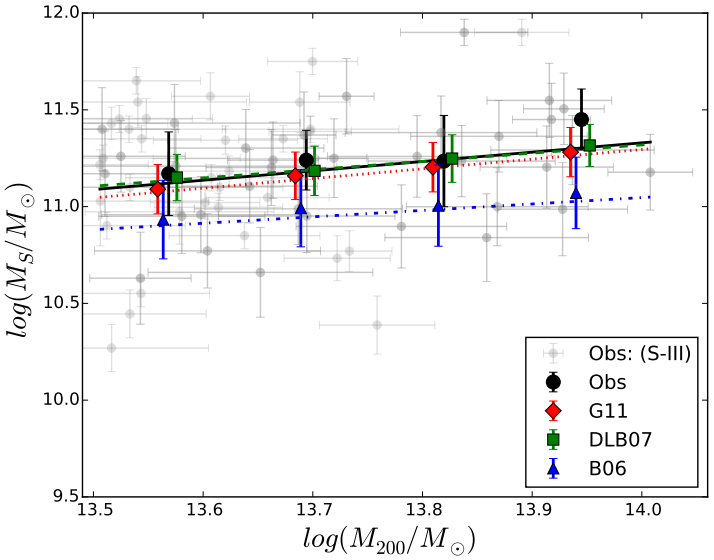

Figure 4.9: The stellar mass of BGGs as a function of the group mass (M_{200}) in observations (gray points). The black points show median stellar mass versus halo mass in observations and the blue, green, and red points show the same in the SAMs of Bower et al. (2006); De Lucia & Blaizot (2007); Guo et al. (2011), respectively. The solid, dashed, dotted and dash-dotted lines represent the best-fitting relations. In agreement with predictions of SAMs, the BGG stellar mass positively correlates with the host group mass. The figure is adopted from Gozaliasl et al. (2016)).

et al. 2010; Collins et al. 2009; Lidman et al. 2012; Oliva-Altamirano et al. 2014).

In contrast, there are some studies that disagree with the strong correlation between halo mass and BCG properties. Guo et al. (2009) studied the relation of the structural parameters of central cluster galaxies with their stellar masses and the host dark matter halo masses. They found that stellar mass of BCGs is the dominant property dictating the shape and size of these objects, and point out that the halo mass plays no significant role, in agreement with findings from Kauffmann et al. (2004); Van Der Wel et al. (2008).

In Gozaliasl et al. (2016), we study the $M_* - M_{200}$ relation for our five subsamples of BGGs. We find a good agreement between the observed relation and the SAM predictions from Bower et al. (2006); De Lucia & Blaizot (2007); Guo et al. (2011). Fig. 4.9 presents this relations in observations (gray points) and SAMs for S-III.

We compare the median stellar mass of BGGs versus the halo mass and the best fit relation between observations and models. Error bars on black and colour points correspond to the median absolute deviation. The solid, dotted, dashed, dash-dotted points show the best fit relations. In agreement with models, we find that the stellar mass of BGGs positively correlates with halo mass of BGGs. Within observational errors, the slope of this relation shows no considerable evolution. We also find that the slope of the $M_* - M_{200}$ relation for BGGs within low-mass haloes (S-I) is steeper than that of the BGGs within massive haloes (S-II) at the same redshift range ($0.04 < z < 0.4$).

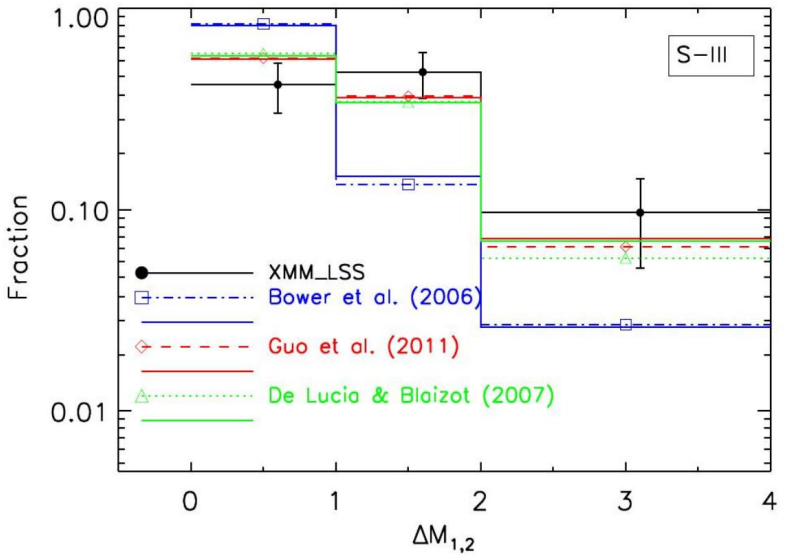

Figure 5.1: Distribution of the magnitude gap of groups at $0.45 < z < 0.80$ in observations (black histogram) and the SAMs. We take into account the effect of contamination in selecting BGGs/brightest satellites with error bars in each bin. The figure is adopted from Gozaliasl et al. (2014a).

5 Magnitude gap and fossil groups

5.1 Magnitude gap

Observations show that gravitational interactions and mergers between group galaxies occur more frequently than in low-density regions. Since the velocity dispersion of group galaxies is sufficiently low, dynamical friction effectively causes massive satellites to dissipate their orbital energy and angular momentum, driving them to

the center of host systems until they eventually merge with the central group galaxy (Chandrasekhar 1943; White 1976a; Ponman et al. 1994). If this is a feasible scenario for the evolution of group galaxies, then the formation and growth of central galaxies are expected to be tightly linked to the evolution of hosting groups. As a result of evolution, the number of the massive galaxies is expected to decrease due to mergers with the central galaxy because the time-scale for major mergers is less than the Hubble time-scale. The changes in the number of dwarf galaxies should be insignificant due to minor mergers, since the time-scale for small galaxy merging is longer. It is expected, due to evolution of group galaxies, that the magnitude differences ($\Delta M_{1,2}$) between the absolute (r-band) magnitude of the central galaxies (M_1) and that of the brightest satellites (M_2) changes.

The luminosity gap or the (r-band) magnitude gap are believed to have physical meaning and they are often used as an optical criterion for determining the group dynamical age, as a diagnostic of past mergers among the massive galaxies in groups, and also as an optical tracer for the cluster mass (e.g., Ponman et al. 1994; Dariush et al. 2007; Hearin et al. 2013). The magnitude gap is also used as an essential parameter for identifying so-called "fossil groups". A fossil group includes a giant elliptical galaxy surrounded with some faint satellites and an extended X-ray emitting hot halo (Ponman et al. 1994; Jones et al. 2003).

In the last two decades, the magnitude gap distribution, relation between group properties (e.g., mass) and the properties of the BGGs/BCGs (e.g., stellar mass, luminosity) have been the focus of several studies (e.g., Dariush et al. 2007; Dariush et al. 2010; Smith et al. 2010; Trevisan et al. 2016). For example, Dariush et al. (2007); Dariush et al. (2010) studied the mass assembly of galaxy groups classified by magnitude gap and found that galaxy groups with large magnitude gaps assemble their mass earlier than the normal groups with small magnitude gaps. Smith et al. (2010) also used SAMs and a sample of 59 massive ($\sim 10^{15} M_{\odot}$) galaxy clusters at $z \lesssim 0.3$ to study the magnitude gap distribution and the properties of groups with large/small magnitude gaps. They found that large magnitude gap clusters are relatively homogeneous including elliptical/disky brightest cluster galaxies (BCGs), cuspy gas density profiles (i.e., strong cool cores), high concentrations and low substructure fractions. Meanwhile small magnitude gap clusters are more heterogeneous. They conclude that the magnitude gap can be used for characterizing clusters and probing model predictions. Recently, Trevisan et al. (2016) find using an SDSS-based sample of 569 groups with elliptical BGGs, that there is no correlation between the magnitude gap of groups and BGG ages and metallicities.

In paper I (Gozaliasl et al. 2014a), we used a catalog of 213 galaxy groups, including 84 groups with spectroscopic membership selected from COSMOS (Finoguenov

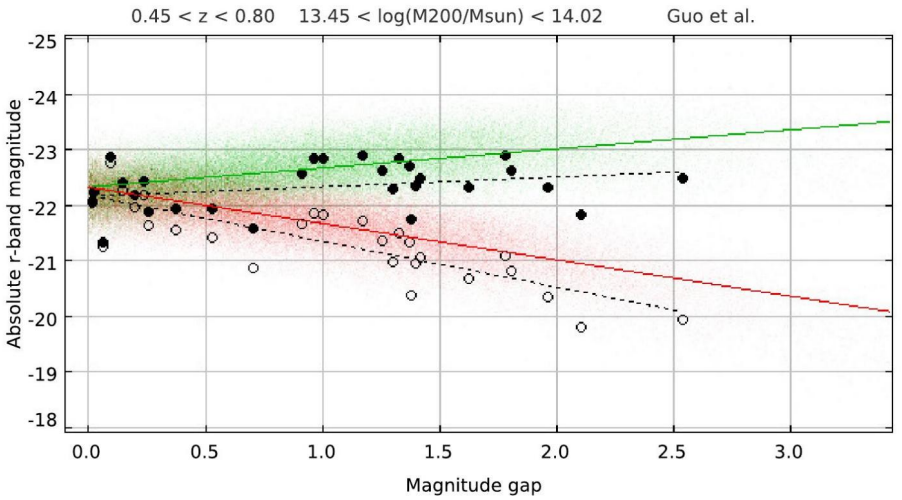

Figure 5.2: Relation between magnitude gap and the absolute magnitude of the BGGs and the second brightest galaxy in observations (black points and lines) and the SAM of Guo et al. (2011) (green and red points and lines). The BGG luminosity increases as a function of increasing magnitude gap. The figure is adopted from Gozaliasl et al. (2014a).

et al. 2007), AEGIS (Erfanianfar et al. 2013), and XMM-LSS (Gozaliasl et al. 2014a) fields in order to extend the study of the magnitude gap distribution and its evolution from $z = 0.3$ out to $z = 1.23$. Fig. 12 in Gozaliasl et al. (2014a) presents the magnitude gap distribution over ~ 9 billion years. Here, Fig. 5.1 shows the magnitude gap distribution for galaxy groups in observations (black histograms) and models (colour histograms) at $0.45 < z < 0.8$. We take into account the effect of contamination by dusty star forming galaxies, effect of completeness, and effect of sample selections in the error bars associated with each magnitude gap bin. As a result, we find that the fraction of groups with large magnitude gaps increases with cosmic time.

In Fig. 16 to Fig. 19 of paper I (Gozaliasl et al. 2014a), we investigate the relation between magnitude gap and absolute r-band magnitude for BGGs and the second brightest group galaxy and compare this relation between observations and the predictions from B06, DLB07 and G11. We also extend this study from $z = 0.3$ out to $z = 1.23$. In Fig. 5.2, we compare this relation between observations and

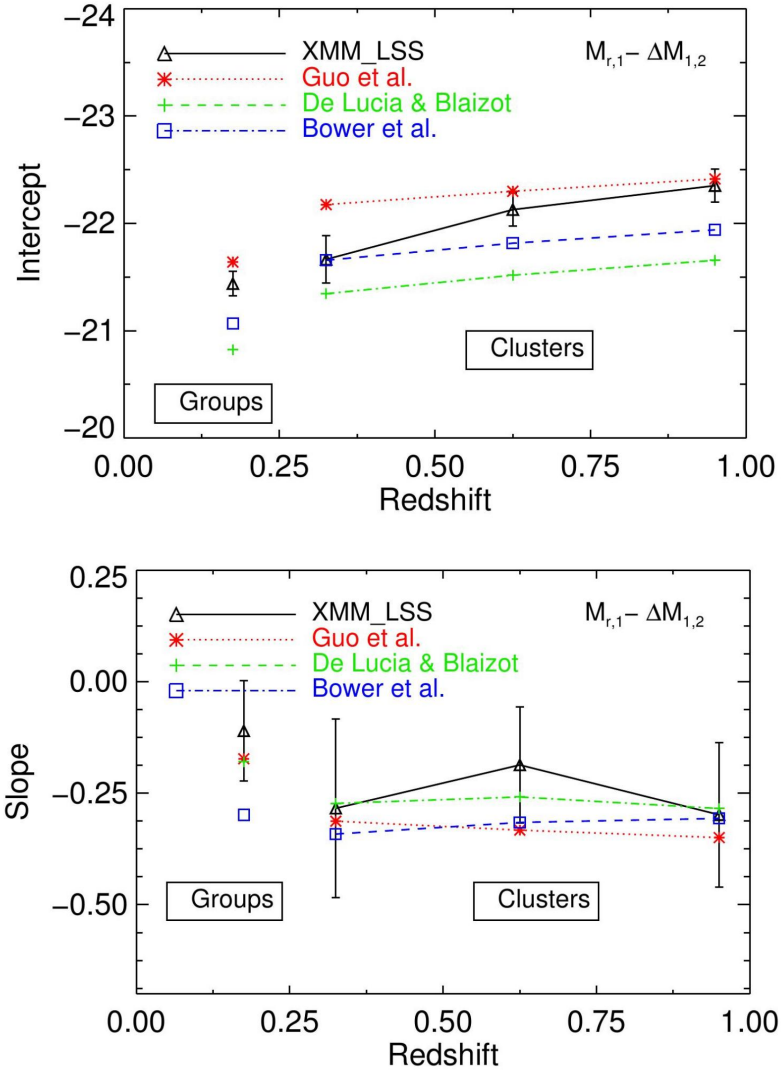

Figure 5.3: Evolution of the zero point and slope of the relation between magnitude gap and r-band absolute magnitude of the BGGs with redshift. The figure is adopted from Gozaliasl et al. (2014a).

the G11 model. We fit the best linear relation to the data in the models (green and red solid lines) and observations (black dotted lines). As a result, we find that

the BGGs of groups with large magnitude gaps are more luminous than those of groups with small magnitude gaps. In Fig. 5.3, the intercept and slope of the best-fit linear relations are plotted as a function of redshift. We show that the zero point of this relation evolves by ~ -1 mag with increasing redshift. We conclude that the high-z BGGs are more luminous than the low-z BGGs within groups with similar halo masses since high-z BGGs are younger than the low-z BGGs. The slope of the relation is found to show no significant evolution in agreement with models.

5.2 Fossil galaxy groups

Numerical simulations (e.g., Barnes 1989) suggest that the end product of merging galaxies in compact groups is a bright giant elliptical galaxy. Observations have also shown that some of the compact groups contain an extended X-ray emitting halo, and thus a considerable amount of dark matter. Therefore, an elliptical galaxy formed, by mergers in these groups will be surrounded by the X-ray emitting halo. Based on these finding, Ponman et al. (1994) used the ROSAT X-ray all sky survey and discovered the first fossil galaxy group. The first formal definition of fossil groups was presented by Jones et al. (2003). According to this definition, a galaxy group is identified as a fossil group if it includes a giant luminous elliptical galaxy with a large r-band magnitude difference ($\Delta M_{1,2} \geq 2$ mag) with the second brightest satellite within half of the virial radius, and also has an extended X-ray emitting hot halo with $L_X \gtrsim 10^{42}$ erg s^{-1}.

The central elliptical galaxies in fossil groups have a significant contribution to the optical appearance of fossil groups. Fig. 5.2 shows the most massive fossil group (RX J1416.4+2315) with $M_h = 3.1 \times 10^{14}$ $M_\odot$ at $z = 0.137$, known to date (e.g., Khosroshahi et al. 2006).

It is believed that fossil groups have formed earlier than other normal groups and clusters and they exhibit no sign of recent major merger and no recent star formation (Jones et al. 2000; Khosroshahi et al. 2007). Using Chandra X-ray data of seven fossil groups, Khosroshahi et al. (2007) studied their X-ray scaling relations and found that fossils contain hotter IGM, more concentrated dark matter, and are more luminous in X-rays than normal groups for a given optical luminosity.

Dariush et al. (2007) show using the Millennium simulation that fossil systems accumulate their mass earlier than non-fossils at high redshifts. The most widely suggested formation scenario for these objects is that dynamical friction causes the massive galaxies close to the core of the group to merge and form the central elliptical with a large magnitude gap (e.g., D'Onghia et al. 2005). Harrison et al. (2012) identified 17 fossil groups and clusters within the XMM Cluster Survey and the Sloan Digital Sky Survey and found that the stellar masses of the BGGs in fossils are larger than those of normal groups at a fixed group/cluster mass. They suggest that fossil galaxy groups have formed early and in the densest regions of the Universe. Bharadwaj et al. (2016) also analyze X-ray observations of 17 fossils and identified most of the fossils as cool-core objects. They contemplate that the AGN feedback and non-gravitational heating could have had an effect on the IGM properties of these objects.

An interesting debate in the literature is whether fossils are a particular class

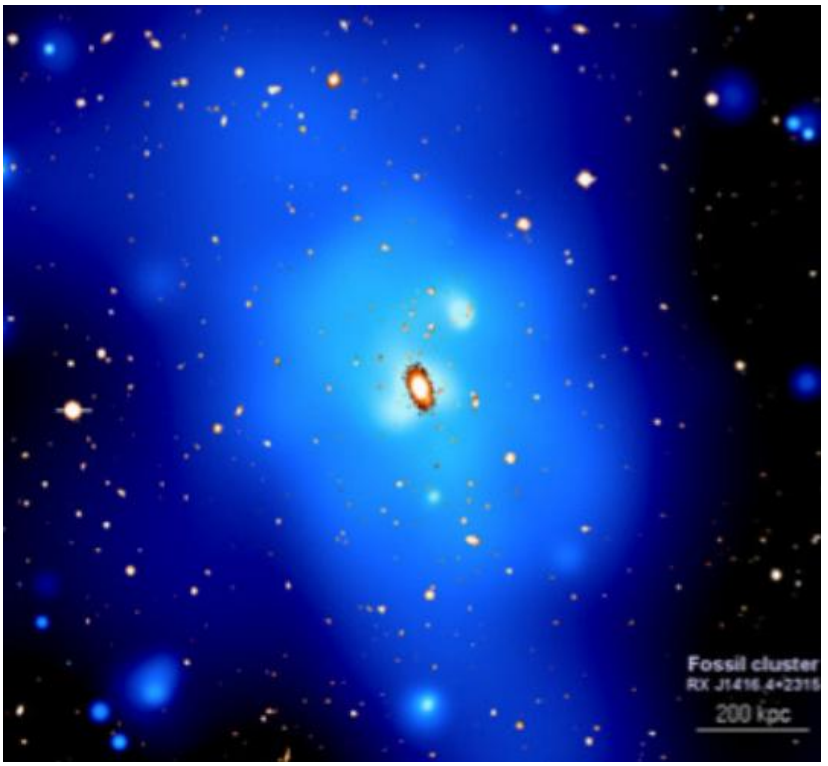

Figure 5.4: The most massive fossil group, RX J1416.4+2315 ($M_h = 3.1 \times 10^{14} M_\odot$) at $z = 0.137$, known to date with extended X-ray emitting (blue) hot gas halo and a giant central elliptical galaxy (Khosroshahi et al. 2006).

of groups representing the end product of galaxy mergers in groups and clusters. La Barbera et al. (2012, 2009) argue that fossil groups are not particular/distinct groups, and merely represent the end stage of mass assembly in a place with insufficient surrounding material. In addition, von Benda-Beckmann et al. (2008) argued using simulation that the large magnitude gap of fossils can be filled by a fresh infall of massive galaxies, thus the fossil phase is temporary.

In this thesis, we identify a large sample of fossils at XMM-LSS, COSMOS, and 2dfGRS and investigate their optical and X-ray properties (Gozaliasl et al. 2014a; Khosroshahi et al. 2014).

In addition, we use the Guo et al. (2011) SAM and trace backwards three subsamples of fossils and non-fossils (BS-I to BS-III as defined in §4.1), from $z = 0$ to $z = 1$,

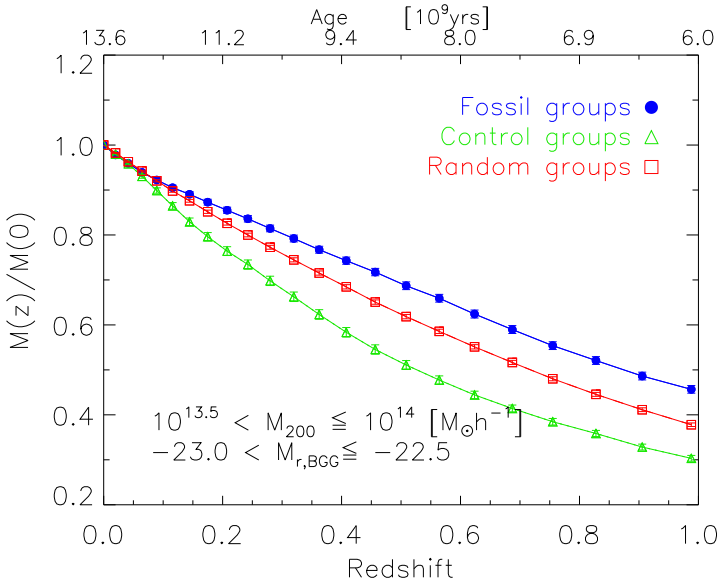

Figure 5.5: The mean halo mass of groups as a function cosmic time. The haloes are selected at $z = 0$ and are traced backwards out to $z = 1$ in the SAM of Guo et al. (2011) model. At $z = 1$, fossils assembled more mass than non-fossils, indicating that they form earlier than non-fossils. The figure is adopted from Gozaliasl et al. (2014b).

and examine whether the galaxy luminosity function, halo mass, and magnitude gap of their progenitors evolve with redshift.

Fig. 5.5 shows the evolution of the halo mass of fossils, controls, and random groups as a function of cosmic time. We find that groups with large magnitude gaps assemble their halo mass earlier than other groups with small magnitude gaps at a fixed redshift (e.g., $z = 1$), indicating that these groups form earlier.

Fig. 5.6 shows the magnitude gap evolution for the haloes that are traced backwards from $z = 0$ to $z = 1$ (upper panel). We also examine the magnitude gap evolution for haloes that are selected at $z = 1$ and are traced forwards from $z = 1$ to $z = 0$ (lower panel). Overall, we find that the magnitude gap of $z = 0$ fossils have significantly grown between $z = 0.6$ and $z = 0$. We also find that the large magnitude gap of $z = 1$ fossils might be filled due to the infall of luminous galaxies.

In Gozaliasl et al. (2014a), we identify a new sample of fossil group candidates in our catalog of X-ray galaxy groups in XMM-LSS and divide them into two subsam-

ples, one including fossils at $z < 0.6$ and the other including fossils at $0.6 < z < 1.23$. We show that the fraction of fossils increases with decreasing redshift by a factor of ~ 2. In addition, we study the colour magnitude diagram of these observed fossils and find evidence that the large magnitude of high-z fossils can be filled by infalling luminous galaxies into the group cores, in agreement with findings in von Benda-Beckmann et al. (2008).

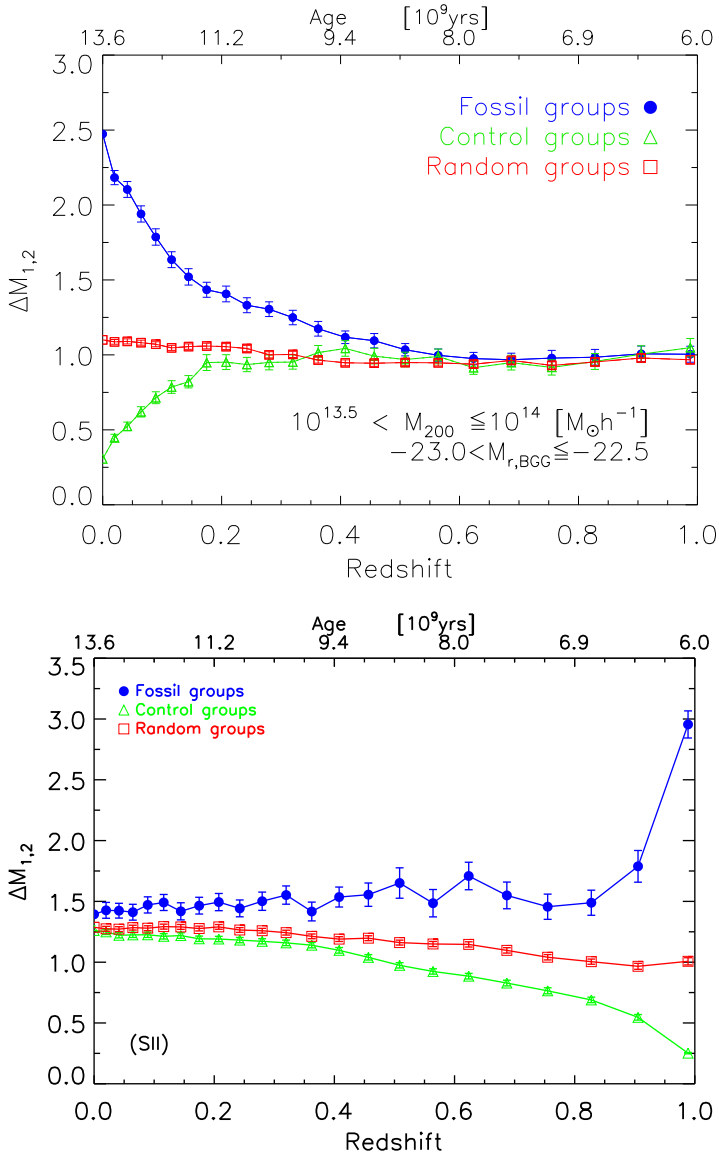

Figure 5.6: *(Upper panel)*Evolution of the magnitude gap of fossil, control, and random groups when they are traced backwards from $z = 0$ to $z = 1$. *(Lower panel)* The same evolution when haloes are traced forwards from $z = 1$ to $z = 0$. This test indicates that the magnitude gap of fossils grows at $z < 0.6$ and a high-z fossil may lose its large gap due to the infall of galaxies. Figures are adopted from Gozaliasl et al. (2014b).

6 Luminosity function of galaxies in group progenitors

The luminosity function of galaxies is well-reproduced by the Schechter luminosity function (Schechter 1976) as follows:

$$\Phi(L) = \left(\frac{\Phi^*}{L^*}\right)\left(\frac{L}{L^*}\right)^{\alpha} \exp(L/L^*), \tag{6.1}$$

where $\Phi(L)dL$ represents the number density of galaxies in the luminosity/absolute magnitude range of [L,L + dL] or [M, M+dM]. The number density of bright galaxies drops exponentially, while the luminosity distribution of faint galaxies change as a power law function with the slope α. L^* defines a characteristic luminosity that separates the two regimes of the bright and faint parts of the luminosity function, and Φ^* has units of number density and represents the normalization of the distribution. Fig. 6.1 shows a schematic plot of the galaxy luminosity function.

The Schechter luminosity function can be written in terms of the absolute magnitude of galaxies (M) as follows:

$$n(M)dM = 0.4ln10\ \phi^*\ \left[10^{0.4(M^*-M)}\right]^{\alpha+1} e^{\left[-10^{0.4(M^*-M)}\right]} dM, \tag{6.2}$$

here, M^* is the characteristic absolute magnitude.

The galaxy luminosity function is a fundamental observable and must be reproduced by successful galaxy formation models. This function has been well studied (e.g., Bahcall 1979; Binggeli et al. 1988; Blanton et al. 2001; Benson et al. 2003; Lin et al. 1996; Popesso et al. 2005; Milosavljević et al. 2006; van den Bosch et al. 2007; Tinker & Conroy 2009). Early studies believed that the luminosity function of galaxies is a universal function and is independent from galaxy properties and their environment (Oemler 1974; Gaidos 1997; Colless 1989; De Propris et al. 2003). In contrast, several studies reveal that the galaxy luminosity function is an environment dependent function (Godwin & Peach 1977; de Filippis et al. 2011; Hansen

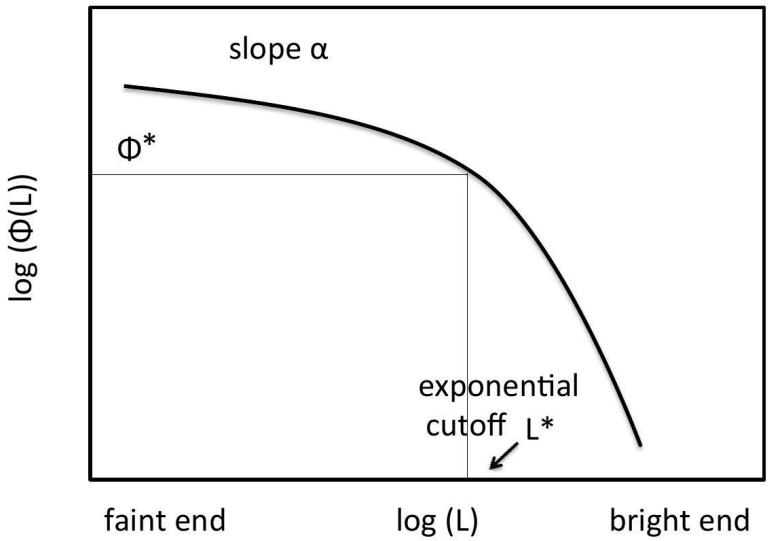

Figure 6.1: A schematic Schechter luminosity function of galaxies with the characteristic luminosity of L^*, a typical faint end slope of α, and corresponding Φ^* (normalization parameter).

et al. 2005; Giodini et al. 2012) changing over cosmic time (Lilly et al. 1995; Ellis et al. 1996; Norberg et al. 2002; Willmer et al. 2006; Alshino et al. 2010; Bowler et al. 2014).

We study the galaxy luminosity function for two purposes. The first is understanding the shape of a single fossil group and the stacked luminosity function of fossil groups within R_{200} and $0.5R_{200}$. The distribution of galaxy luminosities in fossil groups is poorly understood since these systems are very rare. In paper IV (Khosroshahi et al. 2014), we study the luminosity function of some fossil group candidates selected from the Eke et al. (2004) catalog of optically selected galaxy groups in the 2dFGRS field. Fig. 6.2 shows the luminosity function for one of our fossil groups (2PIGG-2868) and the presence of a large magnitude gap at the bright end of its luminosity function.

The second purpose is to test the evolution of the composite (stacked) luminosity function of galaxies in groups classified by a high magnitude gap. The most accepted scenario of formation of the central galaxies in fossil groups suggests that these systems form due to multiple mergers of massive galaxies in a few tenths of a Hubble

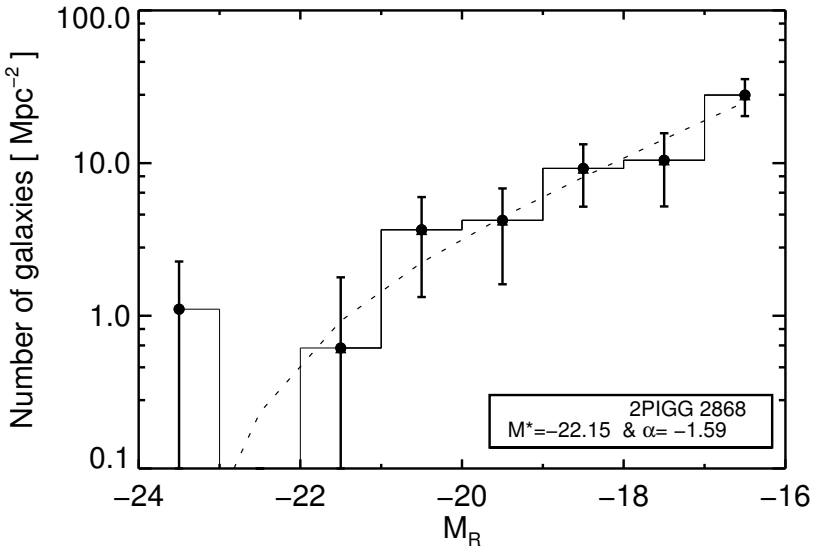

Figure 6.2: The observed composite luminosity function of optically selected fossil groups at $z \sim 0.05$. The figure is adopted from Khosroshahi et al. (2014).

time. For this to be a viable scenario, we expect fossil groups to present a luminosity function with a deficit of L* galaxies. The key lies in the timescale for merging of dwarf galaxies and cooling of the group X-ray halo, which is longer than the period for merging L^* galaxies. Thus, the bright end of the luminosity function of fossils is expected to show stronger time evolution than the faint end slope.

In paper III (Gozaliasl et al. 2014b), we use the SAM of Guo et al. (2011) and define three classes of groups: fossils ($\Delta M_{1,2} \geq 2$ mag), non-fossils/control groups ($\Delta M_{1,2} \leq 0.5$ mag), and random groups (a sample with any $\Delta M_{1,2}$). For each class of groups, we select three subsamples at $z = 0$ (as discussed in §5.2) and we trace them backwards out to $z = 1$. In 23 snapshots and three radii of $0.25R_{200}, 0.5R_{200}$, and R_{200}, we measure the stacked luminosity function of galaxies according to the method presented in Colless (1989) and fit a single Schechter function (Eq. 6.2). Fig. 6.3 shows the stacked luminosity function of fossils within BS-III at $z = 0$.

In Fig. 6.4 and Fig. 6.5, the Schecter parameters α, M^*, ϕ^*, and number of dwarf galaxies are plotted as a function of redshift for subsample BS-II.

In contrast to control groups, we find that M^* for fossils evolves significantly by approximately +1 mag in the last 5 billion years (lower panel in Fig. 6.4). The faint

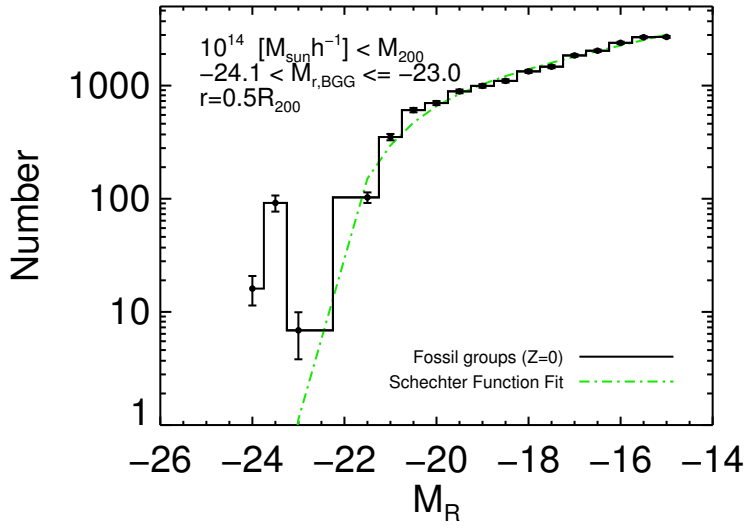

Figure 6.3: The composite (stacked) luminosity function of fossil groups with $M_h > 10^{14} M_\odot$ at $z = 0$ in the SAM of Guo et al. (2011). The large magnitude gap of fossils is seen at the bright end of the luminosity function. The figure is adopted from Gozaliasl et al. (2014b).

end slope shows no significant evolution (upper panel of Fig. 6.4). ϕ^* increases with decreasing redshift for all three classes of groups (upper panel of Fig. 6.5). The number of dwarf galaxies ($-18 \leq M_r < -16$) in fossil groups remains constant over cosmic time in contrast to the significant growth of those for the control and random sample groups (lower panel Fig. 6.5).

Overall, we conclude that the change in ϕ^* for fossils occurs due to the decreasing number of massive galaxies in theses systems. As a result, we argue that central galaxies in fossils mainly form by merging M^* galaxies or major mergers. In addition, since the time scale for merging small galaxies is too long, the minor mergers have a low contribution.

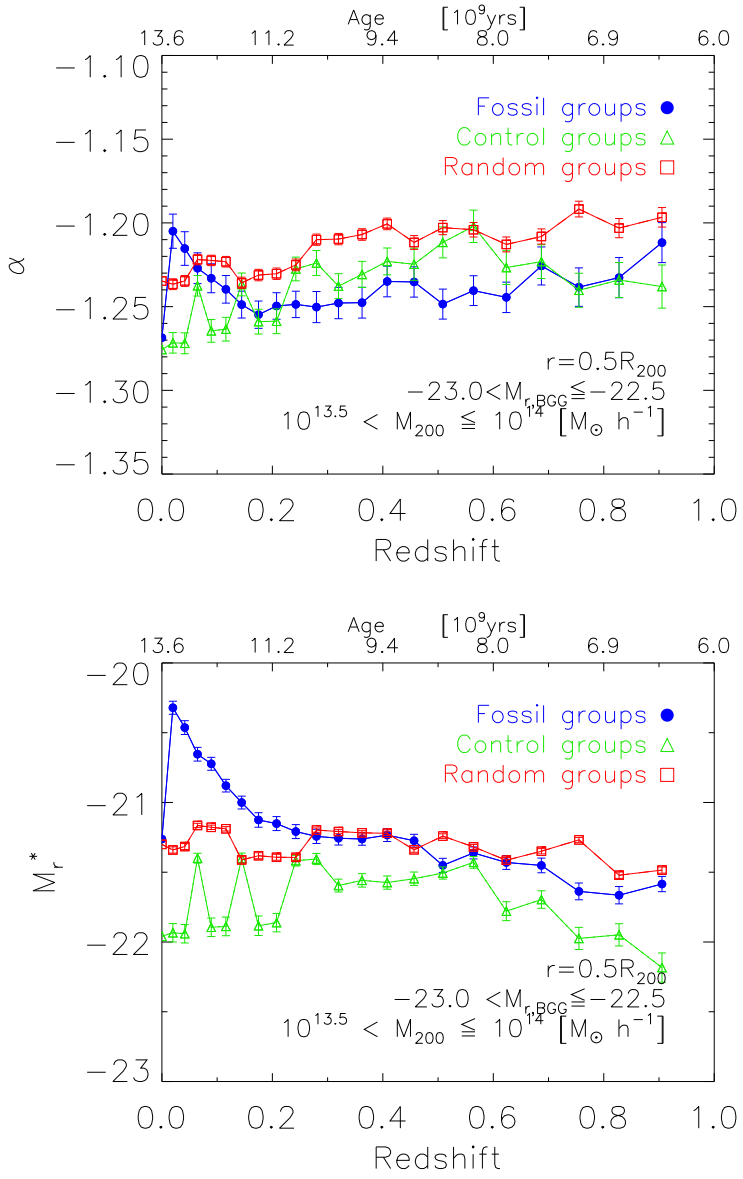

Figure 6.4: *(Upper panel)* Evolution of the faint end slope (α) of the composite luminosity function of galaxies in groups classified by magnitude gap with redshift. *(Lower panel)* Similar plot for the bright end (M^*). M^* for fossils shows a significant growth with redshift by $\sim +1$ mag, while α remains roughly constant for all classes. Figures are adopted from Gozaliasl et al. (2014b).

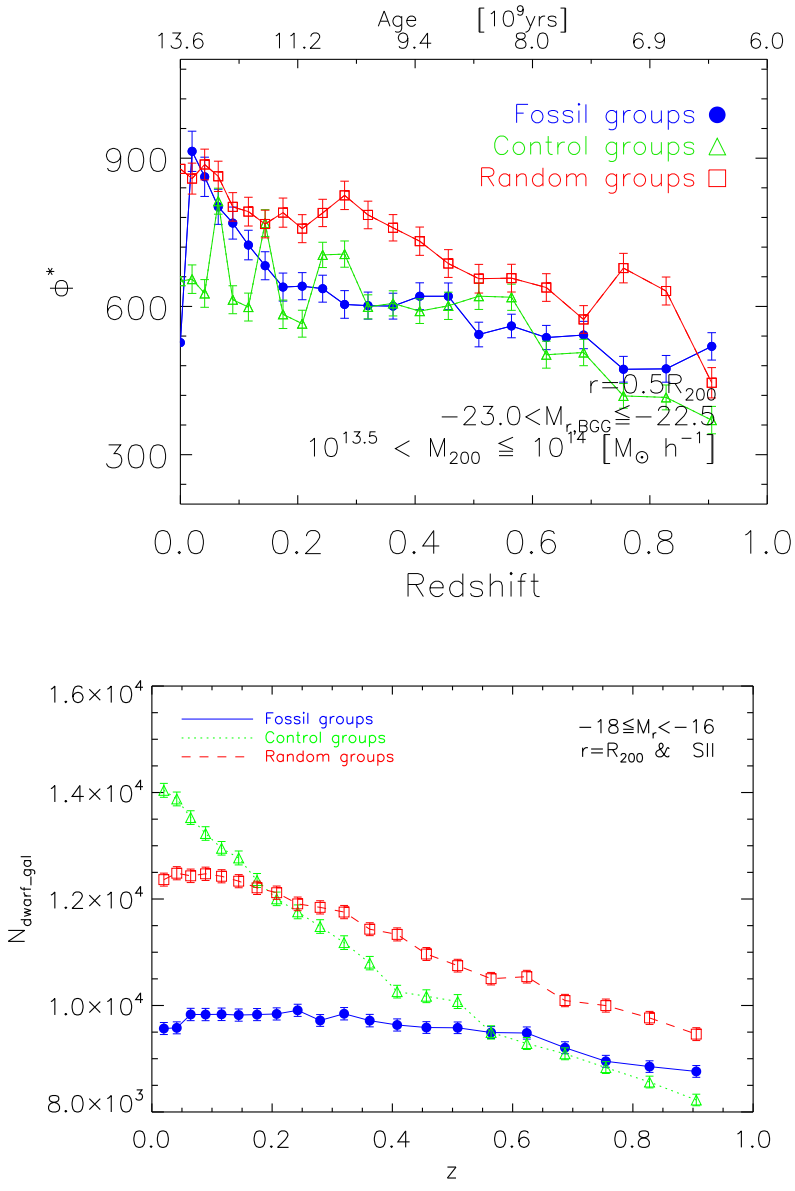

Figure 6.5: *(Upper panel)* Evolution of ϕ^* of the composite luminosity function of galaxies with redshift. *(Lower panel)* Evolution of the number of dwarf galaxies ($-18 \leqslant M_r \leqslant -16$) in groups with redshift. ϕ^* grows significantly for all three classes of groups and the number of dwarf galaxies in fossils remains constant in contrast to other two classes of groups. Figures are adopted from Gozaliasl et al. (2014b).

7 Summary and concluding remarks

In this thesis, we search for the diffuse X-ray emission using the contiguous XMM coverage of the CFHTLS field by the XMM-LSS public data and identify 129 X-ray galaxy groups with $M_{200} = 10^{12.85}$ to $10^{14.2}$ $M_{\odot}$ at $0.04 < z < 1.23$ in the 3 deg^2 CFHTLS-XMM-LSS (Gozaliasl et al. 2014a). We use this data and the data of the X-ray galaxy groups presented in (Finoguenov et al. 2007; Erfanianfar et al. 2013) to address some major goals: the assembly of groups and clusters, the development of the magnitude gap between the BGG and its brightest satellite to assess the use of the magnitude gap as an observable indicator, evolution of the stacked luminosity function of groups classified by magnitude gap, formation of central galaxies in fossils, the distribution and evolution of the stellar mass, and the SFR of BGGs and their relation with halo mass over the last 9 billion years ($0.04 < z < 1.3$). We compare our results with prediction from the SAMs of Bower et al. (2006); De Lucia & Blaizot (2007); Guo et al. (2011); Henriques et al. (2015).

For the first time, we extend the study of the magnitude gap distribution and its relationship with the absolute r-band magnitude of the first and second brightest group galaxies from $z \sim 0.3$ out to $z = 1.23$. Our results suggest that the magnitude gap contains important information on the assembly of groups. We show that galaxy groups with large magnitude gaps such as fossils, are formed earlier than the galaxy groups of similar halo mass with small magnitude gaps at $z = 0$. We also demonstrate that the fraction of galaxy groups with large magnitude gaps increases with cosmic time. As a result, we find the fraction of fossils in observations to grow by a factor of 2 since $z \sim 0.6$. We show that some high-z fossils may lose their large magnitude gap by infalling luminous satellites into the central region ($r < 0.5R_{vir}$) of these systems.

This study shows that the absolute r-band magnitude of BGGs anti-correlates with the magnitude gap, indicating that BGGs in large magnitude gap systems are more luminous than the BGGs in low magnitude gap systems. In addition, the zero point of the relation between absolute r-band magnitude gap of BGGs and magnitude gap is found to evolve by -1 mag as a function of increasing redshift out to $z = 1.23$. We conclude that the high-z BGGs are more luminous than low-z BGGs of haloes

with similar mass due to having younger stellar populations.

We trace backwards haloes classified by the magnitude gap from $z = 0$ to $z = 1$ in the Guo et al. (2011) SAM. We compare the best-fit parameters of the Schechter function to the stacked luminosity function and find that the luminosity function of fossil groups evolves differently compared to non-fossils. In contrast to non-fossils, the M^* parameter of the luminosity function for fossils evolves by at least +1 mag since $z = 1$. The faint end slope (α) shows no significant changes in the luminosity function of all types of groups. While the Φ^* grows significantly for all group classes, indicating that the total number of galaxies in all groups changes with redshift. In addition, the number of dwarf galaxies in fossils is found to remain roughly constant in contrast to the significant growth in non-fossils. These results show that the changes in total number of galaxies in fossils (the changes in Φ^*) are occurring due to changes in the number of massive (M^*) galaxies. We conclude that the central galaxy in fossils must form by merging massive galaxies.

This thesis also investigates, in detail, the evolution of the stellar mass distribution of BGGs within groups of intermediate halo masses ($M_{200} = 10^{12.85}$ to 10^{14} $M_\odot$) at $0.04 < z < 1.3$. We show that the shape of this distribution evolves towards a normal distribution with decreasing redshift in contrast with the SAM predictions. Also in contrast to model predictions, a second peak is detected at the low mass tail of the observed mass distribution at $M_* \sim 10^{10.5}$ $M_\odot$. The galaxies that form the second peak are found to be younger and star forming.

In agreement with SAMs, we show that the average stellar mass of BGGs grows by a factor of 2 since $z = 1.3$ to today. We present observational evidence that this growth becomes slow at $z < 0.5$. Our findings are consistent with recent results for the BCGs of massive clusters (e.g., Lidman et al. 2012; Lin et al. 2013).

We study the evolution and distribution of SFR and sSFR of BGGs and conclude that they are not completely quenched galaxies, since there are a considerable number that continue star formation with rates between 1 and ~ 1000 $M_\odot$ yr^{-1}. The mean SFR of galaxies is found to increase significantly with increasing redshift. The low-mass BGGs are found to be more star forming compared to the massive BGGs at similar redshift. The fraction of star forming BGGs decreases with increasing stellar mass and halo mass in the range probed.

Finally, a positive correlation has been found between the stellar mass of BGGs and the halo mass of their host groups. The slope of the stellar mass and halo mass relation is below unity, concluding that the rate of the stellar mass assembly of BGGs are slower than the rate of the mass assembly of haloes.

This thesis uses multi-wavelength observations of galaxy groups to probe the predictions from several SAMs. We find that the recent modifications in SAMs brings

them much closer to observations than the earlier models, however, they partially fail to reproduce the observations and still need further modifications.

While we know that the contribution of cluster galaxies to the total baryonic mass of clusters is small ($\sim$ 5-15%), understanding the contribution from the central galaxy, satellites, and the ICM to the total cluster baryons can significantly improve cluster modelling. Following this study, we will quantify the contribution of the BCGs/BGGs to the total baryonic mass of cluster/groups. We will estimate the stellar to halo mass ratio for central galaxies as a function of halo mass and the relation between the BGG mass and the halo mass. For the first time, we are quantifying the scatter in the stellar mass of BGGs at a fixed halo mass. The stellar mass assembly of BGGs still needs to be extended to higher redshifts, using high-quality data on group galaxies. In order to achieve this goal, we have begun to confirm spectroscopically our high-z galaxy groups. In addition, we contribute to many ongoing missions of future surveys (e.g., Euclid, eROSITA). These data surveys will provide high-quality data on billions of galaxies and thousands of clusters, which allow us to address precisely the role that environmental and internal physical processes play in the evolution and formation of bright central galaxies in massive haloes.

Bibliography

Adami, C., Mazure, A., Pierre, M., et al. 2011, Astronomy & Astrophysics, 526, A18

Adami, C., Mazure, A., Pierre, M., et al. 2011, Astronomy & Astrophysics, 526, A18

Allen, S., Schmidt, R., Ebeling, H., Fabian, A., & Van Speybroeck, L. 2004, Monthly Notices of the Royal Astronomical Society, 353, 457

Allevato, V., Finoguenov, A., Hasinger, G., et al. 2012, The Astrophysical Journal, 758, 47

Alshino, A., Khosroshahi, H., Ponman, T., et al. 2010, Monthly Notices of the Royal Astronomical Society, 401, 941

Aragón-Salamanca, A., Baugh, C. M., & Kauffmann, G. 1998, Monthly Notices of the Royal Astronomical Society, 297, 427

Ascaso, B., Aguerri, J. A. L., Varela, J., et al. 2011, The Astrophysical Journal, 726, 69

Bahcall, N. A. 1979, The Astrophysical Journal, 232, 689

Balogh, M. L., McGee, S. L., Wilman, D. J., et al. 2011, Monthly Notices of the Royal Astronomical Society, 412, 2303

Barnes, J. E. 1989

Bell, E. F., Wolf, C., Meisenheimer, K., et al. 2004, The Astrophysical Journal, 608, 752

Bellstedt, S., Lidman, C., Muzzin, A., et al. 2016, arXiv preprint arXiv:1605.02736

Benson, A. J. 2010, Physics Reports, 495, 33

Benson, A. J., Bower, R. G., Frenk, C. S., et al. 2003, The Astrophysical Journal, 599, 38

Berlind, A. A., Frieman, J., Weinberg, D. H., et al. 2006, The Astrophysical Journal Supplement Series, 167, 1

Bharadwaj, V., Reiprich, T., Sanders, J., & Schellenberger, G. 2016, Astronomy & Astrophysics, 585, A125

Binggeli, B., Sandage, A., & Tammann, G. A. 1988, Annual Review of Astronomy & Astrophysics, 26, 509

Bîrzan, L., McNamara, B., Nulsen, P., Carilli, C., & Wise, M. 2008, The Astrophysical Journal, 686, 859

Bîrzan, L., Rafferty, D. A., McNamara, B., Wise, M., & Nulsen, P. E. 2004, The Astrophysical Journal, 607, 800

Blanton, M. R., Dalcanton, J., Eisenstein, D., et al. 2001, The Astronomical Journal, 121, 2358

Bleem, L., Stalder, B., De Haan, T., et al. 2015, The Astrophysical Journal Supplement Series, 216, 27

Boehringer, H. & Werner, N. 2009, ArXiv e-prints

Böhringer, H. & Werner, N. 2010, The Astronomy and Astrophysics Review, 18, 127

Bower, R. G., Benson, A. J., Malbon, R., et al. 2006, Monthly Notices of the Royal Astronomical Society, 370, 645

Bowler, R. A. A., Dunlop, J. S., McLure, R. J., et al. 2014, Monthly Notices of the Royal Astronomical Society, 440, 2810

Brimioulle, F., Lerchster, M., Seitz, S., Bender, R., & Snigula, J. 2008, arXiv preprint arXiv:0811.3211

Brimioulle, F., Seitz, S., Lerchster, M., Bender, R., & Snigula, J. 2013, Monthly Notices of the Royal Astronomical Society, 432, 1046

Brinchmann, J., Charlot, S., White, S., et al. 2004, Monthly Notices of the Royal Astronomical Society, 351, 1151

Bromm, V., Yoshida, N., Hernquist, L., & McKee, C. F. 2009, Nature, 459, 49

Brough, S., Collins, C., Burke, D., Mann, R., & Lynam, P. 2002, Monthly Notices of the Royal Astronomical Society, 329, L53

Brough, S., Collins, C. A., Burke, D. J., Lynam, P. D., & Mann, R. G. 2005, Monthly Notices of the Royal Astronomical Society, 364, 1354

Brough, S., Couch, W. J., Collins, C. A., et al. 2008, Monthly Notices of the Royal Astronomical Society, 385, L103

Burke, D., Collins, C., & Mann, R. 2000, The Astrophysical Journal Letters, 532, L105

Capak, P., Aussel, H., Ajiki, M., et al. 2007, The Astrophysical Journal Supplement Series, 172, 99

Chandrasekhar, S. 1943, The Astrophysical Journal, 97, 255

Colless, M. 1989, Monthly Notices of the Royal Astronomical Society, 237, 799

Colless, M., Dalton, G., Maddox, S., et al. 2001, Monthly Notices of the Royal Astronomical Society, 328, 1039

Collins, C., Brough, S., Burke, D., Mann, R., & Lynam, P. 2003, Astrophysics and space science, 285, 51

Collins, C. A., Stott, J. P., Hilton, M., et al. 2009, Nature, 458, 603

Conselice, C. J. 2014, arXiv preprint arXiv:1403.2783

Cox, T., Jonsson, P., Somerville, R. S., Primack, J. R., & Dekel, A. 2008, Monthly Notices of the Royal Astronomical Society, 384, 386

Croton, D. J., Springel, V., White, S. D., et al. 2006, Monthly Notices of the Royal Astronomical Society, 365, 11

Daddi, E., Dickinson, M., Morrison, G., et al. 2007, The Astrophysical Journal, 670, 156

Dai, X., Bregman, J. N., Kochanek, C. S., & Rasia, E. 2010, The Astrophysical Journal, 719, 119

Dariush, A., Khosroshahi, H. G., Ponman, T. J., et al. 2007, Monthly Notices of the Royal Astronomical Society, 382, 433

Dariush, A. A., Raychaudhury, S., Ponman, T. J., et al. 2010, Monthly Notices of the Royal Astronomical Society, 405, 1873

Davis, M., Efstathiou, G., Frenk, C. S., & White, S. D. M. 1985, The Astrophysical Journal, 292, 371

de Filippis, E., Paolillo, M., Longo, G., et al. 2011, Monthly Notices of the Royal Astronomical Society, 414, 2771

de Haan, T., Benson, B., Bleem, L., et al. 2016, arXiv preprint arXiv:1603.06522

De Jager, C., Nieuwenhuijzen, H., & Van Der Hucht, K. 1988, Astronomy and Astrophysics Supplement Series, 72, 259

De Lucia, G. & Blaizot, J. 2007, Monthly Notices of the Royal Astronomical Society, 375, 2

De Propris, R., Colless, M., Driver, S. P., et al. 2003, Monthly Notices of the Royal Astronomical Society, 342, 725

Dennis, T. J. & Chandran, B. D. 2005, The Astrophysical Journal, 622, 205

D'Onghia, E., Sommer-Larsen, J., Romeo, A. D., et al. 2005, The Astrophysical Journal Letters, 630, L109

Dressler, A. 1980, The Astrophysical Journal, 236, 351

Dressler, A., Smail, I., Poggianti, B. M., et al. 1999, The Astrophysical Journal Supplement Series, 122, 51

Dubinski, J. 1998, The Astrophysical Journal, 502, 141

D'Onghia, E., Sommer-Larsen, J., Romeo, A., et al. 2005, The Astrophysical Journal Letters, 630, L109

Eke, V., Baugh, C., Cole, S., et al. 2005, Monthly Notices of the Royal Astronomical Society, 362, 1233

Eke, V. R., Baugh, C. M., Cole, S., et al. 2004, Monthly Notices of the Royal Astronomical Society, 348, 866

Elbaz, D., Daddi, E., Le Borgne, D., et al. 2007, Astronomy & Astrophysics, 468, 33

Ellis, R. S., Colless, M., Broadhurst, T., Heyl, J., & Glazebrook, K. 1996, Monthly Notices of the Royal Astronomical Society, 280, 235

Elvis, M., Civano, F., Vignali, C., et al. 2009, The Astrophysical Journal Supplement Series, 184, 158

Erben, T., Hildebrandt, H., Miller, L., et al. 2013, Monthly Notices of the Royal Astronomical Society, 433, 2545

Erfanianfar, G., Finoguenov, A., Tanaka, M., et al. 2013, The Astrophysical Journal, 765, 117

Fabian, A., Arnaud, K., Bautz, M., & Tawara, Y. 1994, The Astrophysical Journal, 436, L63

Fabian, A. C. & Nulsen, P. E. J. 1977, Monthly Notices of the Royal Astronomical Society, 180, 479

Finoguenov, A., Connelly, J., Parker, L., et al. 2009, The Astrophysical Journal, 704, 564

Finoguenov, A., Guzzo, L., Hasinger, G., et al. 2007, The Astrophysical Journal Supplement Series, 172, 182

Finoguenov, A., Watson, M. G., Tanaka, M., et al. 2010, Monthly Notices of the Royal Astronomical Society, 403, 2063

Font, A. S., Bower, R. G., McCarthy, I. G., et al. 2008, Monthly Notices of the Royal Astronomical Society, 389, 1619

Gaidos, E. J. 1997, The Astronomical Journal, 113, 117

Geller, M. J. & Huchra, J. P. 1983, The Astrophysical Journal Supplement Series, 52, 61

George, M. R., Leauthaud, A., Bundy, K., et al. 2011, The Astrophysical Journal, 742, 125

Gerke, B. F., Newman, J. A., Davis, M., et al. 2012, The Astrophysical Journal, 751, 50

Giodini, S., Finoguenov, A., Pierini, D., et al. 2012, Astronomy & Astrophysics, 538, A104

Glover, S. & Abel, T. 2008, Monthly Notices of the Royal Astronomical Society, 388, 1627

Gobat, R., Daddi, E., Béthermin, M., et al. 2015, Astronomy & Astrophysics, 581, A56

Godwin, J. G. & Peach, J. V. 1977, Monthly Notices of the Royal Astronomical Society, 181, 323

Gozaliasl, G., Finoguenov, A., Khosroshahi, H., et al. 2014a, Astronomy & Astrophysics, 566, A140

Gozaliasl, G., Finoguenov, A., Khosroshahi, H. G., et al. 2016, Monthly Notices of the Royal Astronomical Society, 458, 2762

Gozaliasl, G., Khosroshahi, H., Dariush, A., et al. 2014b, Astronomy & Astrophysics, 571, A49

Gunn, J. E. & Gott III, J. R. 1972, The Astrophysical Journal, 176, 1

Guo, Q., White, S., Boylan-Kolchin, M., et al. 2011, Monthly Notices of the Royal Astronomical Society, 413, 101

Guo, Y., McIntosh, D. H., Mo, H., et al. 2009, Monthly Notices of the Royal Astronomical Society, 398, 1129

Hansen, S. M., McKay, T. A., Wechsler, R. H., et al. 2005, The Astrophysical Journal, 633, 122

Harrison, C. D., Miller, C. J., Richards, J. W., et al. 2012, The Astrophysical Journal, 752, 12

Hasinger, G., Cappelluti, N., Brunner, H., et al. 2007, The Astrophysical Journal Supplement Series, 172, 29

Hattori, M., Kneib, J.-P., & Makino, N. 1999, Progress of Theoretical Physics Supplement, 133, 1

Hearin, A. P., Zentner, A. R., Newman, J. A., & Berlind, A. A. 2013, Monthly Notices of the Royal Astronomical Society, sts699

Henriques, B. M., White, S. D., Thomas, P. A., et al. 2015, Monthly Notices of the Royal Astronomical Society, 451, 2663

Hogg, D. W., Blanton, M. R., Eisenstein, D. J., et al. 2003, The Astrophysical Journal Letters, 585, L5

Hudson, D. S., Mittal, R., Reiprich, T. H., et al. 2010, Astronomy & Astrophysics, 513, A37

Ilbert, O., McCracken, H., Le Fèvre, O., et al. 2013, Astronomy & Astrophysics, 556, A55

Jones, L., Ponman, T., & Forbes, D. A. 2000, Monthly Notices of the Royal Astronomical Society, 312, 139

Jones, L., Ponman, T., Horton, A., et al. 2003, Monthly Notices of the Royal Astronomical Society, 343, 627

Joseph, R. & Wright, G. 1985, Monthly Notices of the Royal Astronomical Society, 214, 87

Kaastra, J., Tamura, T., Peterson, J., et al. 2004, Astronomy & Astrophysics, 413, 415

Kaiser, N. 1986, Monthly Notices of the Royal Astronomical Society, 222, 323

Kang, X. & Van den Bosch, F. C. 2008, The Astrophysical Journal Letters, 676, L101

Kauffmann, G., White, S. D., Heckman, T. M., et al. 2004, Monthly Notices of the Royal Astronomical Society, 353, 713

Kennicutt Jr, R. C. 1998, arXiv preprint astro-ph/9807187

Khosroshahi, H. G., Gozaliasl, G., Finoguenov, A., Raouf, M., & MirAghee, H. 2015, Publication of Korean Astronomical Society, 30, 349

Khosroshahi, H. G., Gozaliasl, G., Rasmussen, J., et al. 2014, Monthly Notices of the Royal Astronomical Society, 443, 318

Khosroshahi, H. G., Maughan, B. J., Ponman, T. J., & Jones, L. R. 2006, Monthly Notices of the Royal Astronomical Society, 369, 1211

Khosroshahi, H. G., Ponman, T. J., & Jones, L. R. 2007, Monthly Notices of the Royal Astronomical Society, 377, 595

Koester, B., McKay, T. A., Annis, J., et al. 2007, The Astrophysical Journal, 660, 239

Kravtsov, A. & Borgani, S. 2012, arXiv preprint arXiv:1205.5556

La Barbera, F., de Carvalho, R., de la Rosa, I., et al. 2009, The Astronomical Journal, 137, 3942

La Barbera, F., Paolillo, M., De Filippis, E., & de Carvalho, R. 2012, Monthly Notices of the Royal Astronomical Society, 422, 3010

Laporte, C. F., White, S. D., Naab, T., & Gao, L. 2013, Monthly Notices of the Royal Astronomical Society, 435, 901

Larson, R. B. 1974, Monthly Notices of the Royal Astronomical Society, 169, 229

Le Fèvre, O., Vettolani, G., Garilli, B., et al. 2005, Astronomy & Astrophysics, 439, 845

Le Fèvre, O., Vettolani, G., Paltani, S., et al. 2004, Astronomy & Astrophysics, 428, 1043

Leauthaud, A., Finoguenov, A., Kneib, J.-P., et al. 2010, The Astrophysical Journal, 709, 97

Leitherer, C., Schaerer, D., Goldader, J. D., et al. 1999, The Astrophysical Journal Supplement Series, 123, 3

Lidman, C., Suherli, J., Muzzin, A., et al. 2012, Monthly Notices of the Royal Astronomical Society, 427, 550

Lilly, S., Le Fèvre, O., Renzini, A., et al. 2007, The Astrophysical Journal Supplement Series, 172, 70

Lilly, S. J., Le Brun, V., Maier, C., et al. 2009, The Astrophysical Journal Supplement Series, 184, 218

Lilly, S. J., Tresse, L., Hammer, F., Crampton, D., & Le Fevre, O. 1995, The Astrophysical Journal, 455, 108

Lin, H., Kirshner, R. P., Shectman, S. A., et al. 1996, The Astrophysical Journal, 464, 60

Lin, Y.-T., Brodwin, M., Gonzalez, A. H., et al. 2013, The Astrophysical Journal, 771, 61

Liu, F., Mao, S., Deng, Z., Xia, X., & Wen, Z. 2009, Monthly Notices of the Royal Astronomical Society, 396, 2003

Liu, F., Mao, S., & Meng, X. 2012, Monthly Notices of the Royal Astronomical Society, 423, 422

Mathews, W. G., Faltenbacher, A., & Brighenti, F. 2006, The Astrophysical Journal, 638, 659

McAlpine, S., Helly, J. C., Schaller, M., et al. 2016, Astronomy and Computing, 15, 72

McCarthy, I. G., Bower, R. G., & Balogh, M. L. 2007, Monthly Notices of the Royal Astronomical Society, 377, 1457

McCracken, H., Milvang-Jensen, B., Dunlop, J., et al. 2012, Astronomy & Astrophysics, 544, A156

McDonald, M., Veilleux, S., Rupke, D. S., Mushotzky, R., & Reynolds, C. 2011, The Astrophysical Journal, 734, 95

McNamara, B. R. & O'Connell, R. W. 1989, The Astronomical Journal, 98, 2018

Merritt, D. 1985, The Astrophysical Journal, 289, 18

Milosavljević, M., Miller, C. J., Furlanetto, S. R., & Cooray, A. 2006, The Astrophysical Journal Letters, 637, L9

Mirkazemi, M., Finoguenov, A., Pereira, M. J., et al. 2015, The Astrophysical Journal, 799, 60

Miyazaki, S., Hamana, T., Ellis, R. S., et al. 2007, The Astrophysical Journal, 669, 714

Mo, H., Van den Bosch, F., & White, S. 2010, Galaxy formation and evolution (Cambridge University Press)

Mok, A., Balogh, M. L., McGee, S. L., et al. 2013, Monthly Notices of the Royal Astronomical Society, 431, 1090

Nelson, A. E., Simard, L., Zaritsky, D., Dalcanton, J. J., & Gonzalez, A. H. 2002, The Astrophysical Journal, 567, 144

Noeske, K., Weiner, B., Faber, S., et al. 2007, The Astrophysical Journal Letters, 660, L43

Norberg, P., Cole, S., Baugh, C. M., et al. 2002, Monthly Notices of the Royal Astronomical Society, 336, 907

Oemler, Jr., A. 1974, The Astrophysical Journal, 194, 1

Oliva-Altamirano, P., Brough, S., Lidman, C., et al. 2014, Monthly Notices of the Royal Astronomical Society, 440, 762

Ostriker, J. & Hausman, M. 1977, The Astrophysical Journal, 217, L125

Ostriker, J. & Tremaine, S. 1975, The Astrophysical Journal, 202, L113

O'dea, C. P., Baum, S. A., Privon, G., et al. 2008, The Astrophysical Journal, 681, 1035

Peebles, P. 1968, The Astrophysical Journal, 153, 1

Pipino, A., Kaviraj, S., Bildfell, C., et al. 2009, Monthly Notices of the Royal Astronomical Society, 395, 462

Ponman, T., Allan, D., Jones, L., et al. 1994, Nature, 369, 462

Popesso, P., Biviano, A., Böhringer, H., Romaniello, M., & Voges, W. 2005, Astronomy & Astrophysics, 433, 431

Postman, M. & Murdin, P. 2001, Encyclopedia of Astronomy and Astrophysics

Prescott, M. K. M., Impey, C. D., Cool, R. J., & Scoville, N. Z. 2006, The Astrophysical Journal, 644, 100

Ramella, M., Boschin, W., Fadda, D., & Nonino, M. 2001, Astronomy & Astrophysics, 368, 776

Raouf, M. & Khosroshahi, H. G. 2015, Publication of Korean Astronomical Society, 30, 363

Raouf, M., Khosroshahi, H. G., & Dariush, A. 2016, The Astrophysical Journal, 824, 140

Reichardt, C., Stalder, B., Bleem, L., et al. 2013, The Astrophysical Journal, 763, 127

Richstone, D. 1976, The Astrophysical Journal, 204, 642

Richstone, D. & Malumuth, E. 1983, The Astrophysical Journal, 268, 30

Rines, K., Finn, R., & Vikhlinin, A. 2007, The Astrophysical Journal Letters, 665, L9

Ruszkowski, M., Brüggen, M., & Begelman, M. C. 2004, The Astrophysical Journal, 611, 158

Sanders, D. & Mirabel, I. 1996, Annual Review of Astronomy and Astrophysics, 34, 749

Sanderson, A. J., Edge, A. C., & Smith, G. P. 2009, Monthly Notices of the Royal Astronomical Society, 398, 1698

Schechter, P. 1976, The Astrophysical Journal, 203, 297

Schneider, P. 2014, Extragalactic astronomy and cosmology: an introduction (Springer)

Scoville, N., Aussel, H., Benson, A., et al. 2007, The Astrophysical Journal Supplement Series, 172, 150

Sijacki, D. & Springel, V. 2006, Monthly Notices of the Royal Astronomical Society, 366, 397

Smith, G. P., Khosroshahi, H. G., Dariush, A., et al. 2010, Monthly Notices of the Royal Astronomical Society, 409, 169

Somerville, R. S., Hopkins, P. F., Cox, T. J., Robertson, B. E., & Hernquist, L. 2008, Monthly Notices of the Royal Astronomical Society, 391, 481

Somerville, R. S., Primack, J. R., & Faber, S. 2001, Monthly Notices of the Royal Astronomical Society, 320, 504

Spergel, D. N., Verde, L., Peiris, H. V., et al. 2003, The Astrophysical Journal Supplement Series, 148, 175

Springel, V. & Hernquist, L. 2005, The Astrophysical Journal Letters, 622, L9

Springel, V., White, S. D., Jenkins, A., et al. 2005, nature, 435, 629

Springel, V., Yoshida, N., & White, S. D. 2001, New Astronomy, 6, 79

Stott, J., Collins, C., Sahlén, M., et al. 2010, The Astrophysical Journal, 718, 23

Stringer, M., Cole, S., & Frenk, C. S. 2010, Monthly Notices of the Royal Astronomical Society, 404, 1129

Sunyaev, R. & Zeldovich, Y. B. 1972, Comments on Astrophysics and Space Physics, 4, 173

Sunyaev, R. A. & Zeldovich, Y. B. 1970, Astrophysics and Space Science, 7, 3

Tamura, T., Kaastra, J., Peterson, J., et al. 2001, Astronomy & Astrophysics, 365, L87

Thomas, D., Maraston, C., Bender, R., & De Oliveira, C. M. 2005, The Astrophysical Journal, 621, 673

Tinker, J. L. & Conroy, C. 2009, The Astrophysical Journal, 691, 633

Tonini, C., Bernyk, M., Croton, D., Maraston, C., & Thomas, D. 2012, The Astrophysical Journal, 759, 43

Toomre, A. 1977, in Evolution of Galaxies and Stellar Populations, Vol. 1, 401

Tremaine, S. D. & Richstone, D. O. 1977, The Astrophysical Journal, 212, 311

Trevisan, M., Mamon, G. A., & Khosroshahi, H. G. 2016, ArXiv e-prints

Trump, J. R., Impey, C. D., McCarthy, P. J., et al. 2007, The Astrophysical Journal Supplement Series, 172, 383

van de Voort, F., Quataert, E., Hopkins, P. F., et al. 2016, arXiv preprint arXiv:1604.01397

Van den Bergh, S. 1976, The Astrophysical Journal, 206, 883

van den Bosch, F. C., Yang, X., Mo, H. J., et al. 2007, Monthly Notices of the Royal Astronomical Society, 376, 841

Van Der Wel, A., Holden, B. P., Zirm, A. W., et al. 2008, The Astrophysical Journal, 688, 48

Vikhlinin, A., Kravtsov, A., Forman, W., et al. 2006, The Astrophysical Journal, 640, 691

Vogelsberger, M., Genel, S., Springel, V., et al. 2014, Monthly Notices of the Royal Astronomical Society, 444, 1518

von Benda-Beckmann, A. M., D'Onghia, E., Gottlöber, S., et al. 2008, Monthly Notices of the Royal Astronomical Society, 386, 2345

Von Der Linden, A., Best, P. N., Kauffmann, G., & White, S. D. 2007, Monthly Notices of the Royal Astronomical Society, 379, 867

Whiley, I., Aragón-Salamanca, A., De Lucia, G., et al. 2008, Monthly Notices of the Royal Astronomical Society, 387, 1253

Whitaker, K. E., Van Dokkum, P. G., Brammer, G., & Franx, M. 2012, The Astrophysical Journal Letters, 754, L29

White, S. D. 1976a, Monthly Notices of the Royal Astronomical Society, 174, 19

White, S. D. 1976b, Monthly Notices of the Royal Astronomical Society, 177, 717

White, S. D., Navarro, J. F., Evrard, A. E., & Frenk, C. S. 1993, Nature, 366, 429

White, S. D. & Rees, M. 1978, Monthly Notices of the Royal Astronomical Society, 183, 341

Willmer, C. N. A., Faber, S. M., Koo, D. C., et al. 2006, The Astrophysical Journal, 647, 853

Wright, N. J., Drake, J. J., & Civano, F. 2010, The Astrophysical Journal, 725, 480

Wuyts, S., Schreiber, N. M. F., Lutz, D., et al. 2011, The Astrophysical Journal, 738, 106

Yoshida, N., Abel, T., Hernquist, L., & Sugiyama, N. 2003, The Astrophysical Journal, 592, 645

Zakamska, N. L. & Narayan, R. 2003, The Astrophysical Journal, 582, 162

Zwicky, F. 1937, The Astrophysical Journal, 86, 217